Habit learning is associated with efficiently controlled network dynamics in naive macaque monkeys

Julia K. Brynildsen 1,† , Panagiotis Fotiadis 1,2,† , Karol P. Szymula 1,3,4,† , Jason Z. Kim 1,5 , Fabio	
$Pasqualetti^{6},AnnM.Graybiel^{7,8},TheresaM.Desrochers^{9,\ddagger,*},andDaniS.Bassett^{1,10,11,12,13,14,\ddagger,*}$	5
¹ Department of Bioengineering, School of Engineering & Applied Science, University of	
Pennsylvania, Philadelphia, PA 19104 USA	
² Department of Neuroscience, Perelman School of Medicine, University of Pennsylvania,	
Philadelphia, PA 19104, USA	
3 Department of Biomedical Engineering, University of Rochester, Rochester, NY 14642 USA	10
⁴ Medical Scientist Training Program, University of Rochester School of Medicine and Dentistry,	
Rochester, New York, USA	
⁵ Department of Physics, Cornell University, Ithaca, NY, 14853, USA	
⁶ Department of Mechanical Engineering, University of California, Riverside, CA 92521 USA	
$^7\mathrm{Mc}$ Govern Institute for Brain Research, Massachusetts Institute of Technology, Cambridge, MA	15
$02139~\mathrm{USA}$	
⁸ Department of Brain and Cognitive Sciences, Massachusetts Institute of Technology,	
Cambridge, MA 02139 USA	
⁹ Department of Neuroscience, Department of Psychiatry and Human Behavior, Robert J. and	
Nancy D. Carney Institute for Brain Science, Brown University, Providence RI 02912 USA	20
$^{10}\mathrm{Department}$ of Electrical & Systems Engineering, School of Engineering & Applied Science,	
University of Pennsylvania, Philadelphia, PA 19104 USA	
$^{11}\mathrm{Department}$ of Physics & Astronomy, College of Arts & Sciences, University of Pennsylvania,	
Philadelphia, PA 19104 USA	
¹² Department of Neurology, Perelman School of Medicine, University of Pennsylvania,	25
Philadelphia, PA 19104 USA	
¹³ Department of Psychiatry, Perelman School of Medicine, University of Pennsylvania,	
Philadelphia, PA 19104 USA	
¹⁴ Santa Fe Institute, Santa Fe, NM 87501 USA	
[†] These three authors contributed equally.	30
[‡] These two authors contributed equally.	
*Corresponding authors: theresa desrochers@brown.edu; dsb@seas.upenn.edu	

Abstract

Primates utilize distributed neural circuits to learn habits in uncertain environments, but the underlying mechanisms remain poorly understood. We propose a formal 35 theory of network energetics explaining how brain states influence sequential behavior. We test our theory on multi-unit recordings from the caudate nucleus and cortical regions of macaques performing a motor habit task. The theory predicts the energy required to transition between brain states represented by trial-specific firing rates across channels, assuming activity spreads through effective connections. 40 We hypothesized that habit formation would correlate with lower control energy. Consistent with this, we observed smaller energy requirements for transitions between similar saccade patterns and those of intermediate complexity, and sessions exploiting fewer patterns. Simulations ruled out confounds from neurons' directional tuning. Finally, virtual lesioning demonstrated robustness of observed relationships between 45 control energy and behavior. This work paves the way for examining how behavior arises from changing activity in distributed circuitry.

Introduction

In a complex ever-changing environment, both humans and non-human primates survive by learning to balance the need to gather new knowledge with the utilization of existing knowledge^{1,2}. The formation of habits can be viewed as a natural consequence of locally optimal trade-offs between exploration and exploitation³. The underlying cognitive processes may follow reinforcement learning algorithms⁴, in which the sampling of actions and the uncertainty of their outcomes inform decisions regarding exploration of new actions or exploitation of old ones⁵. The brain mechanisms supporting such processes engage a distributed set of regions spanning the caudate nucleus associated with repetitive and stereotyped actions⁶, the ventral striatum and amygdala associated with reward and motivation¹, and the prefrontal cortex associated with cognitive control².

Yet, precisely how this constellation of brain regions supports the computations necessary for habits to emerge remains far from understood. Recent efforts suggest that network approaches⁷ provide useful tools for understanding how cognitive processes arise from interacting brain regions⁸. From intelligence to cognitive control, and from motivation to learning, disparate circuits are engaged that allow coordinated information processing and transmission^{9–11}. The study of circuit engagement and function can be formalized in the language of network science¹², and initial evidence suggests that individual differences in the pattern of inter-regional interactions track individual differences in exploratory behaviors and decision-making¹³, plasticity¹⁴, reinforcement learning¹⁵, and skill learning¹⁶. Although network approaches manifest striking face validity, the level of explanation has thus far largely neglected the role of neural connectivity in shaping and constraining patterns of neural activity associated with cognitive and behavioral processes¹⁷.

70

Here we address this challenge by building upon and extending emerging work in the field of network control theory^{18–20}. In the context of neural systems, the approach defines a state of the network to be the vector of regional (or cellular) activation. The theory then posits that the sequence of states is constrained by the energy required to transmute one state into another allowing activity to spread solely through known inter-regional links²¹. In addition to predicting the effects of exogenous control signals such as electrical stimulation²², network control theory has also proven useful in accounting for the intrinsic capacity for cognitive control^{23,24} and the contribution of single neurons to large-scale behaviors²⁵. We extend the approach in two ways. First, prior studies stipulated that activity could only flow along known structural links between regions; here, we instead allow inter-regional links to reflect effective connections²⁶, which represent information flow in the brain during learning^{27,28}. We assume that effective connectivity remains constant over the course of the study and attempt to capture learning-related changes through changes in endogenous inputs. Second, prior studies estimated the energy of brain state transitions independently from behavior; here, we instead explicitly posit (and

validate) the notion that low energy state transitions characterize processes that are less cognitively demanding, as do their associated behaviors²⁹.

We evaluate the theory in the context of multi-unit recordings spanning the caudate nucleus and prefrontal cortex of two macaque monkeys as they engage in 60-180 sessions of task performance inducing motor habits in the form of saccadic patterns³. In each trial, the monkey was presented with a 3×3 grid of green dots and was expected to freely traverse its gaze across the 9 dots (Figure 1). At some variable point during the trial, one of these 9 dots was randomly "baited" unbeknownst to the monkey (the baited target was different across each trial and indistinguishable from the other dots). Once the monkey's gaze entered the baited dot area, the trial ended and a reward was given. Due to the nature of the task, the optimal behavior would thus be for the monkey to perform a sequence of saccadic movements that spanned all dots in a minimal amount of time. We define a brain state to be a vector of firing rates across recording channels within a trial. Further, we construct a neural network whose nodes are channels and whose edges reflect the strength of effective connectivity derived from neural activity time-series; we represent the network as a weighted directed adjacency matrix.

Habits are characterized by repetitive, automatized patterns of behavior. Our primary hypothesis is that pairwise differences in sequential behaviors, as observed across individual trials during habit formation, will be associated with changes in energy requirements of the accompanying neural state transitions. To interpret behavior, we represent saccade 105 patterns as graphs that can be decomposed into 1-D time-series (Figure 2A), whose shape can be studied and whose complexity can be quantified. We observe that preferred saccade patterns change as a function of learning, in a manner that is consistent with the formation of habits. Specifically, we observe increases in the degree of similarity between complex saccade patterns and repetition of stereotypical saccade sequences across 110 time. Using network control theory, we compute the minimum control energy required to transition between chronologically ordered trial brain states where a "state" reflects neural activity across a trial, and may thus reflect activity patterns associated with the behavioral strategy predominantly used within each trial and observe that energy decreases with learning. Finally, we show that the energy of state transitions predicts behavior in three 115 distinct ways: (i) transitioning between more similar saccades patterns requires less energy, (ii) performing saccade patterns of intermediate complexity requires less energy, and (iii) repeatedly exploiting a smaller number of saccade patterns during sessions requires less energy. Together, these findings suggest that lower-energy transitions support behaviors that are less variable and more stereotyped. This pattern is broadly consistent with the 120 principle of maximum entropy, in which energy constraints shape the diversity of accessible behavioral states, as has been observed in other neural and behavioral systems^{30–34}.

To rule out the influence of inherent directional tuning properties of neurons, we conducted simulations using only the monkeys' saccadic trajectories, excluding recorded

firing rates. Unlike the empirical variables, the correlations in the simulated variables were either non-significant or much weaker, indicating that directional tuning did not drive our results. Lastly, we aimed to identify which parts of the brain's connectome contribute most to the relationship between control energy and saccadic performance. We perform virtual lesion analyses, setting connectome edges to zero. Edges whose knockout renders the relationship non-significant are deemed critical. We find that disrupting most edges is required for our observed behavior-energy correlations to become non-significant. Taken together, our work represents a theoretically principled study of habit learning that identifies a relationship between transitions in behavior and the energetics of transitions in neural states.

Results

The data analyzed in this work consist of neural recordings and behavioral measurements from two female macaque monkeys, Monkey G (60 recorded sessions; 9,702 task trials) and Monkey Y (180 recorded sessions; 80,664 task trials), while performing a free-view scanning task. All data were previously collected and reported^{3,6}. Neural data were recorded from approximately 100 electrodes implanted in the caudate nucleus, Brodmann 140 areas 8 (frontal eye fields), 9 (dorsolateral and medial prefrontal cortex), 13-14 (insula and ventromedial prefrontal cortex), 24-25 (anterior and subgenual cingulate), and 45-46 (pars triangularis and middle frontal area). As depicted in Figure 1, at the beginning of each trial the monkey is shown a 3×3 grid of green targets on a screen and allowed to visually navigate the grid-space freely. At a variable time, one of the targets is baited 145 without the monkey's knowledge. When the monkey's gaze enters the baited target space, the green grid is replaced by smaller gray circles (marking the end of the task trial) and the monkey receives a reward after a short delay On average, each trial lasted $6.2 \pm 1.1 \text{ s}$ (mean \pm SD) for MG and 8.0 ± 1.3 s for MY. Within trials, the scan epoch (from scan_on to scan off) lasted 1.9 ± 1.1 s for MG and 2.2 ± 1.2 s for MY, and the reward delivery 150 epoch (reward on to reward off) lasted 0.20 ± 0.002 s for MG and 0.29 ± 0.06 for MY.

Earlier analyses of this dataset^{3,6} indicate that both monkeys showed evidence of learning over repeated trials, with increasingly efficient visits to the targets within each trial and more repetitive saccade patterns (i.e., decreased saccade entropy) across sessions, regardless of the pattern being performed. A reinforcement learning algorithm closely mirrored this behavior. However, while the reward rate—measured as the number of rewards earned per total scan time—remained relatively constant for Monkey G and reached asymptote for the last 18 sessions for Monkey Y, the monkeys' scan patterns continued to evolve well beyond this point³. These results suggest that scan time alone may not effectively capture habit formation, as changes in scan time did not consistently align with the monkeys' shifting approach to the task.

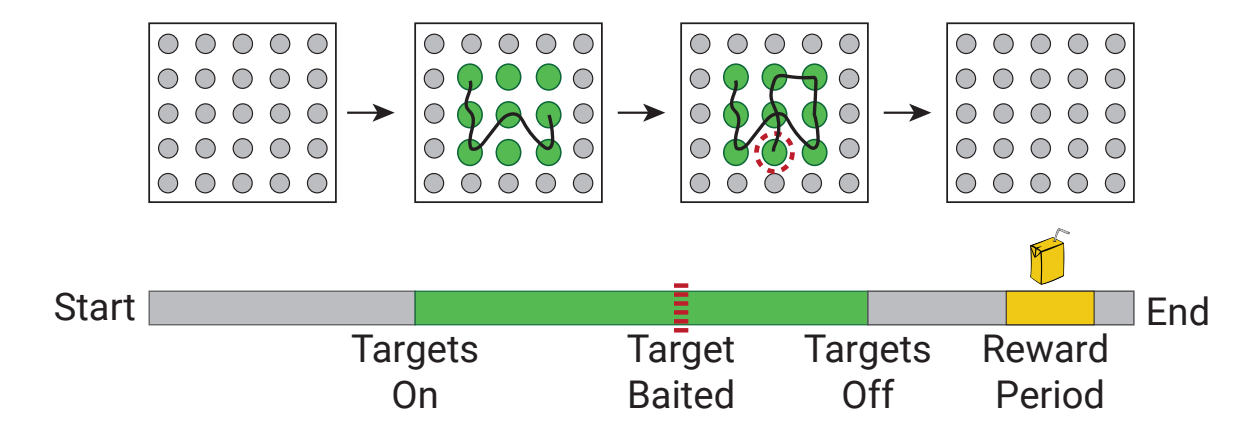


Figure 1: The Free Scan Task. A visual depiction of a single trial from the free scan task. The trial begins (Start) with a grid of small grey dots all equally sized and spaced. A 3×3 grid of larger green targets replaces the central part of the gray grid $(Targets\ On)$. The monkey is allowed to freely scan the space of green targets. At a variable time unknown to the monkey, a target is baited $(Target\ Baited)$. For visualization purposes in the context of this exposition, the baited target is depicted surrounded by a red dashed circle; note that the outline is not present during the actual task. When the monkey's gaze enters the baited target, the grid of green targets disappears and is replaced by all gray targets $(Targets\ Off)$. After a brief variable delay, a liquid reward is given to the monkey $(Reward\ Period)$ after which the trial is considered finished (End).

Classification of Trial Representative Saccade Patterns

Behavioral measurements were analyzed in the form of trial-specific chronological saccade sequences performed by a monkey during the task. We use the phrase $individual\ saccade$ to refer to a rapid eye movement from one target to another on the task grid. The phrase 165 $saccade\ sequence$ then refers to a series of individual saccades that are performed one after another. Direct qualitative or quantitative comparison between the trial-specific saccade sequences is difficult due to variability in trial length and, as a result, the number of saccades per trial. Therefore, we first set out to arrange the list of individual saccades into a format that allows for interpretable comparison between trials. We began by converting each trial's saccade sequence into an adjacency matrix of a directed and weighted graph, G(N, E), where N is the number of nodes (one for each green grid target) and E is the set of all edges that exist between nodes (Figure 2A). An edge between two nodes exists if a saccade was observed between the two specific grid targets. Furthermore, the weight of each edge is the total number of times the specific saccade is performed during the trial. 175 We refer to this representation of the trial saccades as the $saccade\ network$.

Saccade patterns that create *loops* (or sequences that start and end on the same target) in which each target is visited only once before returning to the starting target are the most effective strategies since they allow for an efficient and organized approach to scanning the 3×3 grid space³. Indeed, the majority of successful trials for each monkey 180 (75.96% for MG and 74.64% for MY) were comprised of looping sequences, underscoring

their development as the dominant strategy in successful task performance. Accordingly, we identified the most observed cyclic saccade pattern in each trial by leveraging the concept of network paths (see Methods). A series of edges that is traversed to move from one node in the network to another is called a path. In a saccade network, a path represents a set of observed saccades performed one after another. If the path's start node is the same as the path's end node then the path is cyclic and the represented saccade sequence is a loop. For each trial, we therefore defined the trial representative saccade pattern (TRSP) to be the cyclic path in the trial saccade network with the greatest sum of edge weights (Figure 2A). Intuitively, the TRSP is the cyclic sequence of saccades that was performed most frequently during a trial; see Supplementary Figure 1 for a graphical depiction of TRSP identification.

Methods for computing the similarity between 1-D signals are numerous, easy to implement computationally, and provide simple intuitive understanding. Therefore, to make the comparison between TRSPs as simple as possible we converted each pattern into a 1-D saccade waveform (Figure 2A). This dimensionality reduction step was made possible by representing the identified TRSP as a series of (x, y) points in the space of the task grid and calculating each points' Euclidean distance from the centroid of all points. We take the similarity between any two trial saccade patterns to be a metric based on the Euclidean distance between the trial saccade waveforms (see Methods). We use this metric to group all the trials into clusters of saccade patterns based on their similarity to each other. Since the exact number of present clusters in the data was not known, the agglomerative clustering algorithm was used to group TRSPs (Figure 2B). This algorithm starts by treating each object (i.e. saccade pattern) as a single cluster and uses an iterative process to merge pairs of objects into clusters until all objects are grouped into one large cluster. The output of the algorithm is a dendrogram (cluster tree) which depicts the order in which objects should be grouped during clustering.

In order to capture more natural divisions of our data during clustering, we used the inconsistency coefficient which is a useful metric in agglomerative clustering that compares the height of a link in a cluster tree to heights of all the other links underneath 210 it in the tree. A small coefficient denotes little difference between the objects being grouped together, thereby suggesting that the clustering solution is a good fit to the data. Examining a range of inconsistency coefficient values allowed us to identify an optimal threshold criterion for clustering. Setting a threshold on the inconsistency coefficient during clustering enables the identified groupings to more closely represent the natural 215 divisions found in the data. Using the elbow-method and the average within cluster sum-of-squares from a range of inconsistency coefficient thresholds (0.1-1.5, in intervals of 0.05), we selected an inconsistency coefficient of 0.95 to be the optimal threshold criterion for clustering. As a result, a total of 136 clusters were identified for Monkey G and 346 for Monkey Y; see Supplementary Figures 2 and 3 for a full tabulation. In Figure 2C, 220

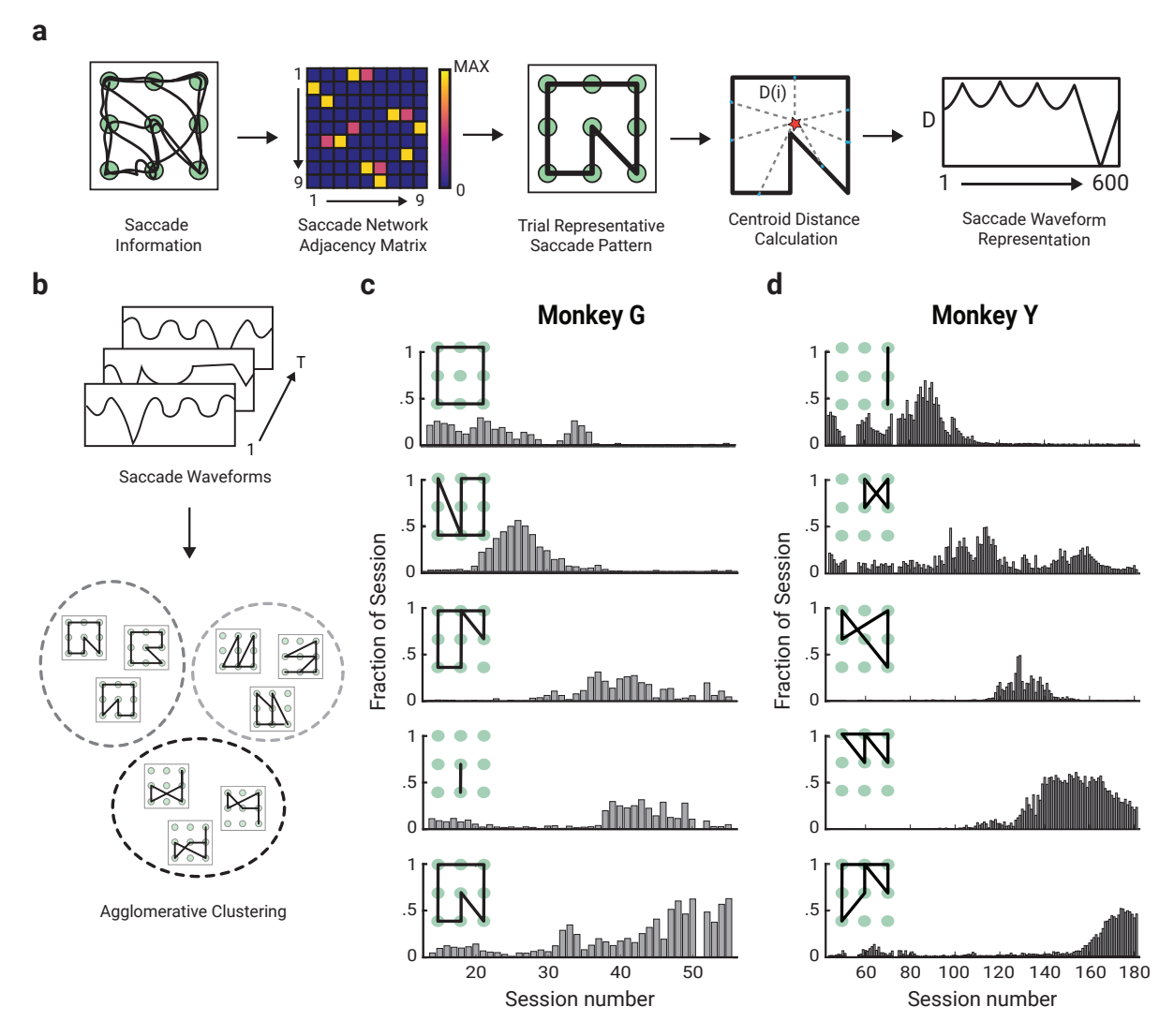


Figure 2: Classification of Trial Representative Saccade Patterns. information in the form of identified saccadic movements during a trial is collectively represented as an adjacency matrix, which in turn encodes a directed and weighted network. A total of nine nodes exist: one for every green target on the task grid. Edge weights are calculated as the number of times that an individual saccade is made from one node to another. The network is converted into a trial representative saccade pattern by identifying the network cycle with the greatest sum of edge weights along its path. Each TRSP is treated as a 2-D polygon in the task grid space consisting of a set of (x,y) points. The saccade waveform is taken to be the vector of Euclidean distances between the polygon centroid and all of its points. A 1-D interpolation is performed to reduce each saccade waveform to 600 values. (b) A dissimilarity matrix is constructed utilizing the saccade waveforms from all observed trials. Each element in the dissimilarity matrix is the Euclidean distance between two saccade waveforms. The dissimilarity matrix is of size $T \times T$ where T is the total number of trials for a given monkey. Agglomerative clustering with a threshold inconsistency coefficient of 0.95 was performed using the dissimilarity matrix to cluster all trial saccade waveforms. For Monkey G, we identified a total of 136 cluster whereas for Monkey Y, we identified a total of 346 clusters. (c,d) The five most prevalent cluster saccade patterns across all sessions are shown for each monkey. The saccade pattern shown is the one which is most similar to all other saccade patterns in the same cluster.

the five most prominent TRSPs for each monkey as well as their appearance frequency distribution across all sessions are shown. These patterns and their dynamics closely resemble those previously reported³. Both monkeys demonstrate non-uniform distributions of cluster appearance frequencies across sessions. Each of the main cluster types is acquired, preferentially performed, and dropped at varying time windows throughout the task.

225

Inferring Effective Connectivity

After quantitatively characterizing behavior, our next aim was to demonstrate that pairwise differences in sequential saccade patterns during habit formation can be explained by the energy requirements of the accompanying neural state transitions. We approached the problem by using and extending recent advances in network control theory^{18–20}. 230 Fundamental to any control energy analysis is knowledge of the network structure and dynamics. Thus, as a first step we extract a network of interactions between the observed regions from available channels (Figure 3A). In both monkeys, more than half of the present channels were associated with the caudate nucleus and recordings from Brodmann area 8 (BA-8) were available in both. Although the anatomical location of each channel 235 was known, no information regarding their anatomical connectivity was available and we therefore turned to alternative inference approaches²⁶.

Specifically, we inferred the effective connectivity of the regions using their neural activity (see Methods). For each session, the activity of the available channels was calculated as the firing rate during each individual trial. This set of trial firing rates was 240 used to calculate the transfer entropy³⁵ between all pairs of available channels, which provides basic topographical information about the effective connectivity between them (Figure 3B). The effective connectivity matrices for Monkey G and Monkey Y are displayed in (Figure 3C, 3D).

Assessing the Control Energy Required for Neural State Transitions 245

In applying and extending network control theory to understand habit formation, our next step is to use the effective connectivity networks to estimate the energy requirement of neural state transitions. We use the concept of minimum control energy from control theory, which represents the minimum amount of input energy necessary to cause a network to transition from a specific initial state of activity to a specific final state of activity (Figure 4A)²². Intuitively, the more energy a transition requires, the more difficult it is to reach the final state. In the context of neural systems, control energy has previously been found to correlate with cognitive effort^{24,29}.

In prior work, minimum control energy has been defined for mechanical and technological systems, or abstract mathematical models. To use the approach here, we must first identify a relevant dynamical model for the considered network process. This model consists of (i)

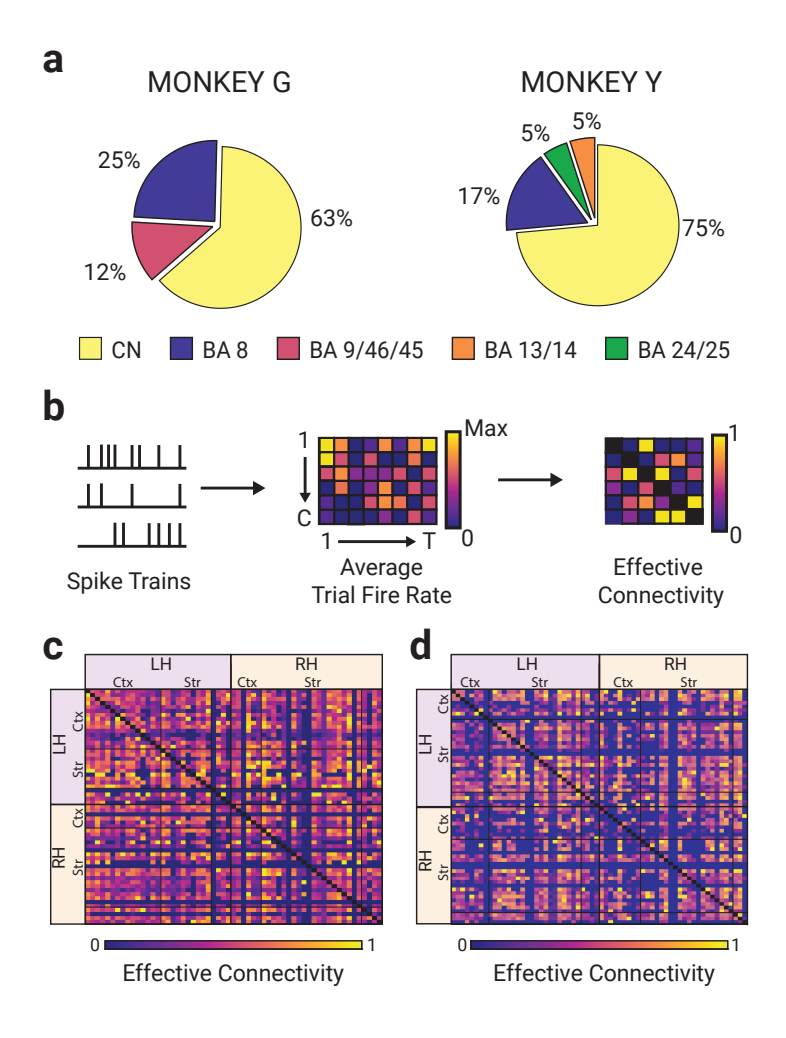


Figure 3: Inferring Effective Connectivity from Neural Activity. (a) Summary of channel recording regions for both monkeys. Percentages denote the percent of all available channels which record from a given region across all trials. CN = caudate nucleus; $BA 8, 9, 13-14, 24-25, 45-46 = Brodmann areas 8 (frontal eye fields), 9 (dorsolateral and medial prefrontal cortex), 13-14 (insula and ventromedial prefrontal cortex), 24-25 (anterior and subgenual cingulate), and 45-46 (pars triangularis and middle frontal area). (b) Spike trains from all channels for a given session were converted into a trial firing rate matrix. The matrix is of size <math>C \times T$, where T is the number of trials for a session and C is the number of available channels during the session. We used transfer entropy³⁵ to estimate the effective connectivity between session channels. (c,d) The overall combined effective connectivity matrices for both monkeys are shown where channels are organized according to their respective hemispheres (LH = Left; RH = Right). Both matrices are individually normalized column-wise by dividing each column by its maximum value; normalization was performed for visualization purposes only. Ctx: Cortex; Str: Striatum.

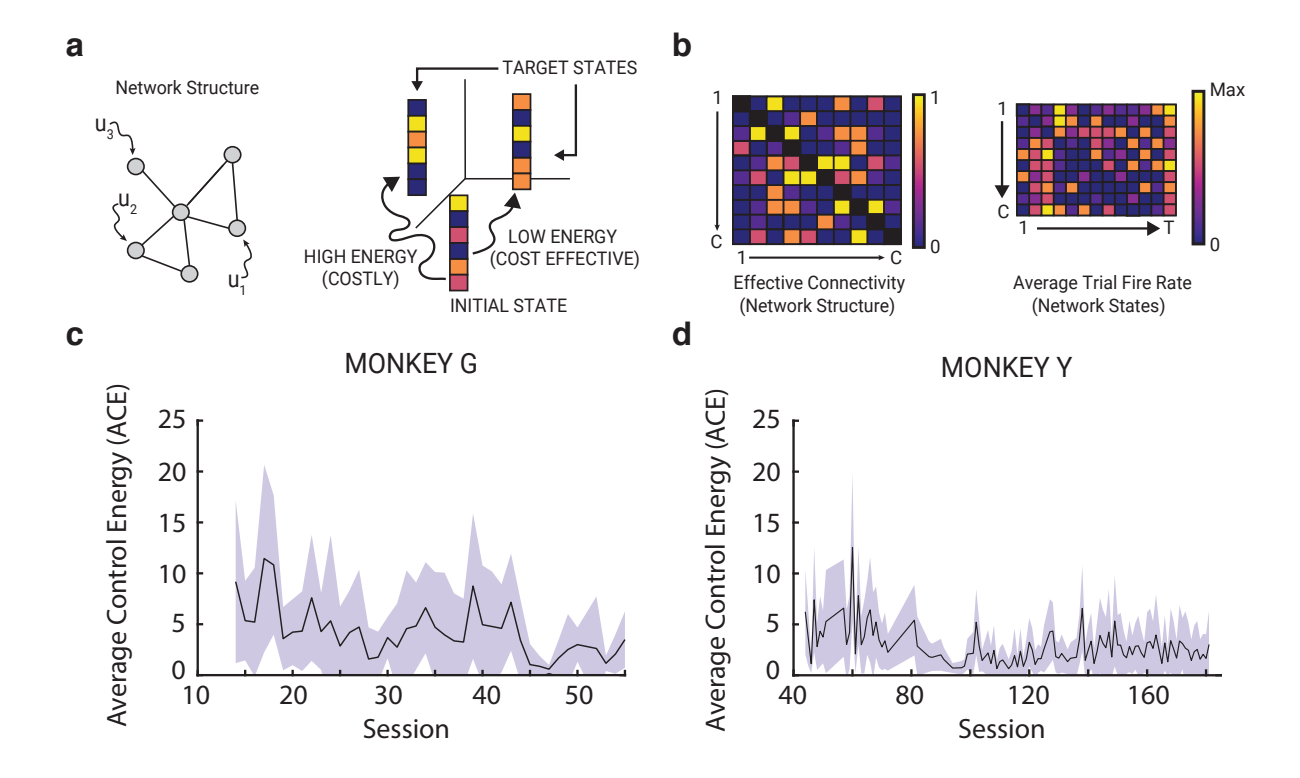


Figure 4: Estimating the Minimum Control Energy to Transition between Neural States. (a) Visual depiction of control energy analysis. Given a network, the goal is to identify a set of time-dependent inputs (e.g., $u_1(t)$, $u_2(t)$, and $u_3(t)$) into network nodes that drives the system from an initial state to a target state in a fixed period of time. A state is a $1 \times N$ vector x_t whose elements represent the activity of each of N nodes in the network at some time t. The calculation of minimum control energy estimates the energy required to transmute one state into another allowing activity to spread solely through known inter-regional links. The greater the minimum control energy the more costly and hard-to-reach that target state is said to be. (b) For a given session, we model the network of channels as a linear time independent system and compute the minimum control energy required to transition between chronologically ordered trial states. A trial state is taken to be the firing rate of each channel over the course of an entire trial. The topology of the network is defined by a session-based subset of the weighted average matrix, in which nodes vary across sessions depending on channel availability, and effective connections between them are consistent. (c-d) The average minimum control energy (ACE) is calculated across all pairwise trial state transitions of a particular session. ACE dynamics for both monkeys across their respective sessions are shown. Filled boundary areas represent ± -1 standard deviation.

a network state, which we define as the trial firing rates (Figure 4B), (ii) a transition map for the state, which we define as the inferred effective connectivity matrix, and (iii) a set of driver nodes, which include all the nodes in our study (see Methods). Edges within the effective connectivity matrix represent the average of the set of non-zero connections 260 between each pair of channels across all sessions in which both of those channels were available (see Methods). With these variables defined, we then estimate the energy required to transmute one state into another allowing activity to spread solely through effective connections. Specifically, we calculated the average minimum control energy (ACE) theoretically required for the observed trial-to-trial state transitions within each 265

session (see Methods).

Effective connectivity matrices were computed for each session and then averaged across sessions to obtain an overall effective connectivity matrix. For both monkeys, effective connectivity covariance increased across sessions (Monkey G: $f_{statistic} = 38.8$, $p = 2.78 \times 10^{-7}$; Monkey Y: $f_{statistic} = 32.6$, $p = 1.04 \times 10^{-7}$). A significant negative 270 correlation between effective connectivity covariance and ACE was observed for Monkey G ($f_{statistic} = 16.2$, $p = 2.65 \times 10^{-4}$ but not for Monkey Y Supplementary Figure 6). To mitigate the potential impact of channel variability across sessions, we chose to use the overall effective connectivity matrix rather than session-specific effective connectivity matrices for all control computations presented in the main text. We note that for 275 MY, our ability to infer region-specific influences on network dynamics is limited by the variability in channel availability across sessions. For MG, all regions included in the analysis (CN, BA-8, and BA-9/45/46) were represented in all sessions. For MY, CN channels were available in 100.00% of sessions, BA-8 channels were available in 97.27% of sessions, BA24/25 channels were available in 17.27% of sessions, and BA13/14 channels 280 were available in 9.09% of sessions.

The ACE dynamics of both monkeys follow a similar downward trend throughout the entire experiment (Figure 4C, 4D). This finding is consistent with the notion that control energy reflects cognitive effort^{24,29}; increasingly habitual behavior requires decreasing levels of cognitive control. A simple linear regression confirmed that there was a statistically 285 significant negative relationship between ACE and session (Monkey G: $\beta = -0.1141$ (95% CI [-0.1703, -0.0578]), $R^2 = 0.30$, $p = 1.98 \times 10^{-4}$; Monkey Y: $\beta = -0.0157$ (95% CI [-0.0235, -0.0080]), $R^2 = 0.13$, $p = 1.06 \times 10^{-4}$). We note that the distributions of ACE across sessions differed significantly between the two monkeys, even after downsampling MY's dataset to match the size of MG's dataset (p = 0.0025926). Differences in data 290 distribution could contribute to the differences in the strength of the relationship between ACE and session.

Notably, the drop in ACE across sessions as well as the correlations between ACE and other saccade metrics remained particularly robust across a range of different time horizons (0.5 to 1.5, in increments of 0.25; **Supplementary Figure 4**). These relationships were 295 also robust to simulated increases in network size. We recomputed the energy cost associated with transitioning between each pair of brain states after simulating networks of 25, 100, 200, or 1,000 additional nodes for each monkey and embedded the original network in each of these simulated networks. The relationships between ACE and session and between ACE and saccade metrics persisted in the presence of additional nodes, 300 suggesting that the results reported here hold when the circuit under study is embedded in a wider network (Supplementary Figure 5).

Though significant, we note that correlations between ACE and session were relatively low (Figure 4C, 4D). We believe this may be attributable to several factors. We expect

that decreases in ACE underlie increases in habitual behavior, which does not increase in a perfectly linear fashion over time. Fluctuations in learning, and therefore in the control energy for neural state transitions, could be attributable to day-to-day fluctuations in motivational state. Daily fluctuations in motivation may be attributable to changes in internal state, including fluctuations in satiety³⁶.

310

Relating the Control Energy to Saccades

We next sought to quantitatively characterize how the monkeys' approaches to the free-scanning task changed over time. For this purpose, saccade patterns were characterized according to three metrics: the similarity factor (SF), complexity factor (CF), and cluster label entropy (CLE). These metrics were chosen because they reflect key properties of optimal habitual behavior: automatization and efficiency³⁷. More specifically, the SF 315 reflects the repetitiveness of saccade patterns over trials, such that increased similarity may be understood to represent increased automatization as habitual behavior is acquired. The CF, or complexity of a saccade pattern, is inversely related to scan efficiency which increases with habit formation. Finally, the CLE reflects the degree of randomness with which the monkeys chose to perform particular saccade patterns. It is inversely related to scan repetitiveness which is associated with habitual behavior. Below we will discuss results for each metric in turn.

The first metric, the SF, represents the similarity between two TRSPs performed consecutively within the same session (see Methods). This metric can be used to answer the question, "Is the monkey performing increasingly similar patterns the longer she 325 engages in the task?". The higher the value of this metric, the more similar the saccade patterns between trials. It is important to note that this metric was designed to be orientation-independent and reflection-independent. Accordingly, the SF renders two instances of the same pattern as identical even if one was rotated, the patterns were exact mirror images of each other, or rotations of exact mirror images (see **Supplementary 330 Figure 7**). This feature of the similarity metric is shown in (Figure 5a), where patterns 3 and 5 only differ in their orientation but result in a SF of approximately 1. As hypothesized, the average SF persistently increased the longer the monkeys engaged with the task (Monkey G: $\beta = 0.0018$ (95% CI [0.0005, 0.0032]), $R^2 = 0.17$, p = 0.0077; Monkey Y: $\beta = 0.0013$ (95% CI [0.0011, 0.0014]), $R^2 = 0.71$, $p = 1.6 \times 10^{-30}$; **Supplementary 335 Figure 8a**).

Although the range of similarity values across task sessions for both monkeys was the same (0.55 to 0.80), the ASF distribution of Monkey Y is skewed towards higher values (Figure 5d). A two-way Kolmogorov-Smirnov test confirmed that the ASF distributions of the two monkeys were significantly different from each other ($ks_{stat} = 0.3541$, $p = 340 \cdot 7.57 \times 10^{-4}$). Furthermore, the Pearson correlation between the ASF and ACE (for

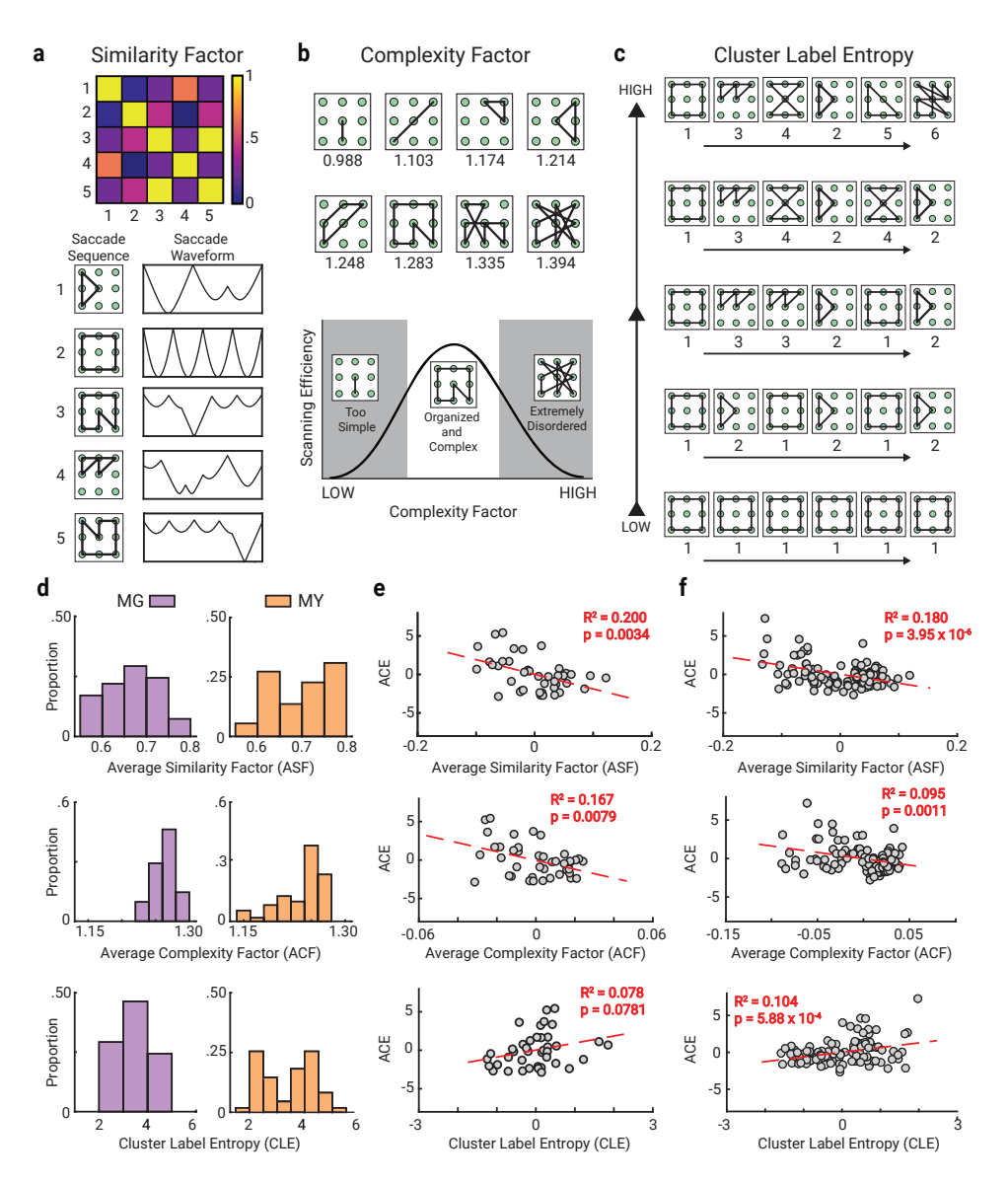


Figure 5: Relating Control Energy to Saccades. (a) The similarity factor (SF) captures information about the similarity between chronologically ordered trial saccade patterns. The similarity between two trial representative saccade patterns is calculated as a metric based on the Euclidean distance between two saccade waveforms. Here we show a visual depiction of 5 example patterns performed by the monkeys, their respective saccade waveform representations, and their similarity to one another. (b) The complexity factor (CF) is calculated as the fractal dimension of the saccade pattern. A range of observed patterns and their CFs are shown. Both extremely low and extremely high complexity patterns result in poor scanning efficiency during the task. (c) The cluster label entropy (CLE) metric captures information about the monkey's preference towards exploration of various patterns or exploitation of only a select few during a task session. The CLE is calculated as the Shannon entropy of the vector of identified trial cluster labels from a single session. Higher values indicate preference for constantly exploring a variety of clusters with minimal exploitation of any single cluster. (d) Side-by-side comparison of saccade metric distributions across all sessions for both monkeys. The average similarity and average CFs were calculated on a per-session basis. (e-f) Linear correlations between all average saccade metrics and the average minimum control energy (ACE) for Monkey G (e) and Monkey Y (f), after adjusting for the number of channels in the recorded regions. The Coefficient of Determination (R^2) and p-value are provided for each plot. Each point represents one session.

Monkey G, r = -0.447, $p = 3.4 \times 10^{-3}$; for Monkey Y, r = -0.424, $p = 3.95 \times 10^{-6}$) was significantly negative in both monkeys, after adjusting for the number of channels in the recorded regions (Figure 5e, 5f). Permutation tests were performed independently for each monkey, to ensure that the observed associations between ASF and ACE were due to the 345 observed neural circuit architecture (see Methods). The observed correlations between ASF and ACE for both monkeys proved to be significantly more negative than expected in their respective permutation null distributions (for Monkey G, $p < 10^{-3}$; for Monkey Y, $p < 10^{-3}$). On the basis of these results, we conclude that decreasing minimum control energy requirements are associated with the performance of increasingly similar saccade 350 patterns.

In contrast to the SF, which captures repetitiveness, the second metric, the CF, quantifies the complexity of an individual TRSP within a session, defined as the fractal dimension of the pattern (see Methods). The metric can be used to answer the question, "Is the monkey approaching the task in a strategic way or is it simply saccading at random?" 355 Both extremely low and extremely high complexity values are not optimal strategies for scanning the task grid efficiently. A pattern with a low complexity (≈ 1) is often too simple and does not cover all the targets in the task. In contrast, a saccade pattern of high complexity (i.e., greater than 1.3) is extremely disordered, tortuous, and seemingly random without any strategy (Figure 5B). Patterns that strike a balance between organization 360 and complexity offer the most efficient approach to scanning the 3×3 target grid.

Both monkeys performed saccade patterns of similar complexity throughout their respective trials, with most sessions averaging to values between 1.24 and 1.28 (Figure 5d). However, the full range of complexity that Monkey Y exhibited was larger than that exhibited by Monkey G, as Monkey Y spent several sessions performing markedly simple patterns. Indeed, Monkey Y's average CF (ACF) increased over time ($\beta = 0.0006$ (95% CI [0.0005, 0.0007]), $R^2 = 0.55$, $p = 1.79 \times 10^{-20}$; Supplementary Figure 8b). A two-way Kolmogorov-Smirnov test confirmed that the ACF distributions of the two monkeys were significantly different from each other ($ks_{stat} = 0.4581$, $p = 3.75 \times 10^{-6}$). Furthermore, the Pearson correlation between the ACF and minimum control energy (for Monkey G, 370 $r = -0.409, p = 7.9 \times 10^{-3}$; for Monkey Y, $r = -0.307, p = 1.1 \times 10^{-3}$) was significantly negative in both monkeys, after adjusting for the number of channels (Figure 5e, 5f). Permutation tests were performed independently for each monkey, to ensure that the observed associations between the ACF and ACE were due to the observed neural circuit architecture (see Methods). The observed correlations between the ACF and ACE for 375 both monkeys proved to be significantly more negative than expected in their respective permutation null distributions (for Monkey G, $p < 10^{-3}$; for Monkey Y, $p < 10^{-3}$).

Finally, the third metric, the CLE, is a quantitative estimate of a monkey's preference towards pattern exploration or exploitation during a task session. It is a direct calculation of Shannon's information entropy of the vector of chronologically ordered trial cluster labels

380

in an individual session. The higher the CLE of a session, the less ordered the behavior and the more prone the monkey was to explore a variety of different saccade patterns coming from multiple identified clusters. The metric can be used to answer the question, "Is the monkey choosing to explore many different saccade patterns across trials or does it continuously exploit a select few?" Over time, both monkeys persistently decreased their 385 CLE, exploiting a smaller number of saccadic patterns as the sessions went by (Monkey G: $\beta = -0.0491$ (95% CI [-0.0615, -0.0367]), $R^2 = 0.62$, $p = 8.78 \times 10^{-10}$; Monkey Y: $\beta = -0.0170$ (95% CI [-0.0198, -0.0141]), $R^2 = 0.56$, $p = 3.74 \times 10^{-21}$; Supplementary Figure 8c).

The distribution of CLE for Monkey Y across sessions shows that she exhibited 390 moments of both extreme exploitation (CLE = 2-3) and extreme exploration (CLE = 4-5.5). In contrast, Monkey G exhibited a preference for mid-range values of CLE with a majority of the task sessions falling in the range of 3-3.5, a balance between exploitation and exploration (Figure 5d). A two-way Kolmogorov-Smirnov test confirmed that the CLE distributions of the two monkeys were not significantly different from each 395 other ($ks_{stat} = 0.2020, p = 0.1539$). The Pearson correlation between the CLE and minimum control energy (for Monkey G, r = 0.278, p = 0.0781; for Monkey Y, r = 0.323, $p = 5.88 \times 10^{-4}$) was significantly positive in Monkey Y only, after adjusting for the number of channels (Figure 5e, 5f). Permutation tests were performed independently for each monkey, to ensure that the observed associations between cluster entropy and 400 ACE were due to the observed neural circuit architecture (see Methods). The significant correlation between CLE and ACE found in Monkey Y proved to be significantly more positive than expected from the respective permutation null distribution (for Monkey G, p = 1; for Monkey Y, $p < 10^{-3}$).

As noted above, Kolmogorov-Smirnov tests revealed significant differences in ASF 405 and ACF (p < 0.001 for both), indicating that the monkeys exhibited distinct behavioral tendencies. Despite these differences, the relationship between ACE and each behavioral measure was consistent in direction across monkeys (Figure 5), suggesting a common underlying association. The observed distributional differences likely contribute to the variation in model fit statistics (e.g., R^2 values) between monkeys, and we highlight them 410 here to aid interpretation of individual differences described throughout the manuscript.

A hallmark of habit learning is a reduction in the cognitive load associated with performing the same behavior. To assess whether similar behavioral patterns become less costly over the course of learning in this task, we identified pairs of behavioral patterns with the same complexity factor that occurred in both early and late sessions for each monkey. For each matched pair, we obtained the control energy associated with the neural state transition between the two patterns for both early and late sessions. When a given transition occurred multiple times within an epoch (early or late), we averaged the control energy across all instances, yielding one value per transition type per epoch. This analysis

revealed that the energy cost of transitioning between matched pairs was significantly 420 lower in later sessions compared to earlier sessions for both monkeys (MG: t(226) = 4.0612, $p = 6.733 \times 10^{-5}$; MY: t(824) = 6.657, $p = 5.110 \times 10^{-11}$; Supplementary Figure 11), where the reported degrees of freedom correspond to the number of unique transition types observed in both early and late epochs. This finding is consistent with the interpretation that, over the course of training, transitions between similar behavioral states become 425 more energetically efficient, reflecting reduced neural control demands. Such a reduction is a hallmark of habitual, automated behavior, and thus these results directly support our claim that habit learning in this task is accompanied by reduced cognitive load.

Lastly, to ensure that there was no significant bias introduced by using the same sequence of spikes to infer both effective connectivity and control energy across sessions, 430 we repeated the correlational analyses reported in this section by inferring effective connectivity on the first half of each session's trials and ACE on the remaining trials (Supplementary Analysis 3). Our results remained virtually identical. Taken together, all aforementioned results suggest individual differences in the distribution of exploitative and exploratory behaviors, yet a consistent direction of the relationship between these 435 strategies and minimum control energy across monkeys, even though not all relationships reached statistical significance in both animals.

Simulation Analysis

Given that neurons found in the brain areas examined in this work have been found to display directional tuning ^{38,39}, and provided that neurons' directional tuning can affect their 440 firing rates depending on the directionality of saccadic movements in space (as in the case of a grid), we performed a simulation to ensure that our main results reported in the previous sections are not driven by directional tuning alone. This was particularly important in our study since the neurons' firing rates were used to generate the effective connectivity matrices that were then used to compute the control energy metrics. In brief—and as 445 explained in further detail in Methods—we generated "null" effective connectivity matrices for each Monkey using only the Monkey's saccadic movements and not her measured firing rates; these matrices were then used to compute each Monkey's "simulated" average minimum control energy. We first examined how each Monkey's simulated average control energy changed over sessions. Even though there was a significant negative correlation 450 between the empirically-measured ACE and session progression, the relationship between the simulated ACE and session progression was not significant (Monkey G: $\beta = -0.061$ (95% CI [-0.136 0.015]), $R^2 = 0.063, \, p = 0.1122; \, \text{Monkey} \, Y \colon \, \beta = \text{-0.005} \, (95\% \, \, \text{CI} \, [\text{-0.015}] \,)$ [0.006]), $R^2 = 0.008$, p = 0.3613).

We next compared the simulated ACE with the empirically-derived ASF. There was 455 once again a lack of association between the two variables for both Monkeys (for Monkey G,

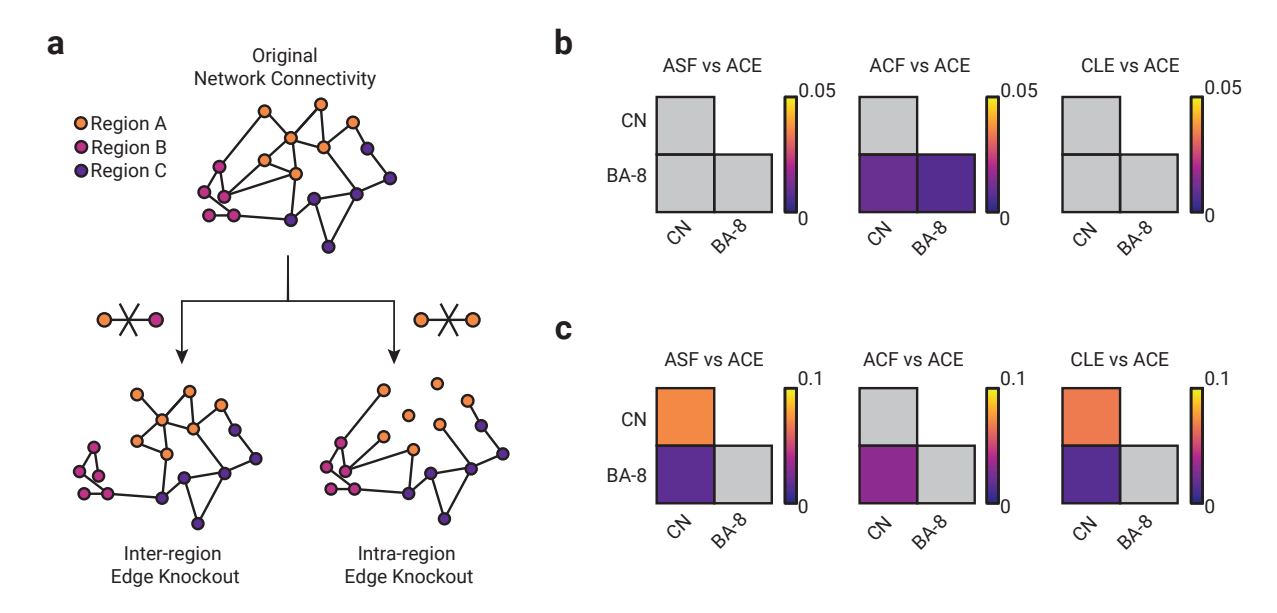


Figure 6: Virtual Region Specific Lesion Analysis. (a) Visual depiction of lesion analysis workflow. The lesion knockout consists of performing a series of edge-knockouts where (i) all edges between two regions are set to zero in the effective connectivity matrix (inter-region), or where (ii) all edges connecting one region to itself are set to zero (intra-region). The average minimum control energy is then calculated using the lesioned effective connectivity matrix, and correlations are computed between the average minimum control energy and all saccade metrics. (b-c) Results of lesion analysis across regions of the CN and BA-8 for Monkey G (b) and Monkey Y (c). All post-lesion correlations were compared to an equivalent null distribution constructed from random edge lesions. Matrix elements represent the absolute value difference between post-lesion and pre-lesion correlations. All grayed out edges represent lesions which did not result in a significant change in correlation value when compared to their respective null distribution. ASF: Average Similarity Factor; ACF: Average Complexity Factor; CLE: Cluster Label Entropy; ACE: Average Control Energy; CN: Caudate Nucleus; BA: Brodmann Area

r=-0.233, p=0.1430; for Monkey Y, r=-0.179, p=0.0607), indicating that directional tuning alone could not explain the significant association reported between the empirical variables. Repeating these analysis between the simulated ACE and ACF, we found that there was no association between the two variables in one of the two monkeys (Monkey G, 460 r=-0.280, p=0.0767). Even though the association between ACF and the simulated ACE remained significant for the other Monkey (Monkey Y, r=-0.275, p=0.0037), the effect size was notably lower than that between the empirical variables. Lastly, we compared the simulated ACE with the CLE and found no significant correlation between the two variables in both Monkeys (for Monkey G, r=0.159, p=0.3222; for Monkey Y, r=0.115, p=0.2317). Collectively, these results lend support to the notion that directional tuning alone could not explain the significant associations reported between the empirical variables.

Identifying Neural Substrates Particularly Key to the Relation Between Control Energy and Saccades

470

In a final step, we seek to determine which part(s) of the inferred network of brain regions significantly contribute to the observed relationships between control energy and behavior. We do so by performing a virtual lesion analysis consisting of a series of interor intra-region edge knockouts in the inferred effective connectivity matrix (see Figure 6A and Supplementary Figure 9 for a schematic depiction of this approach). An edge 475 knockout refers to setting the weights of edges in the effective connectivity matrix to a value of zero, thereby virtually removing connections in the network. Edges whose knockout serves to remove the correlation (resulting in a p-value greater than $\alpha = 0.05$) between ACE and saccade metrics are inferred to be important in controlling task specific energy dynamics. If the correlations can be removed by localized edge deletions, then 480 we would infer that the energetic constraints on neural state transitions are localized to a particular part of the circuit. If instead the correlations cannot be removed by localized edge deletions, then we would infer that the energetic constraints on neural state transitions are broadly distributed across the circuit.

We first performed inter-region and intra-region edge knockouts across all possible 485 combinations of brain regions for each monkey. Inter-region edge knockouts consisted of setting all edges between two regions to zero in the effective connectivity matrix, while intra-region edge knockouts consisted of setting all edges connecting one region to itself to zero. The results are shown in Figure 6B and Figure 6C. In Monkey G, the removal of connections between BA-8 and BA-9/45/46 resulted in small but significant changes to 490 the originally observed correlation between the control energy and the ASF as well as the ACF. In Monkey Y, the removal of connections within the caudate nucleus resulted in small but significant changes to the originally observed correlation between the control

energy and both the ASF and CLE. Although significant changes were found in both monkeys, none were drastic enough to fully disrupt the observed correlations between 495 behavior and control energy.

In order to directly assess the relative importance of inter- versus intra-region knockout, we performed 1,000 virtual knockouts of 500 random inter-region edges and 1,000 virtual knockouts of 500 random intra-region edges, computed the change in correlation between ACE and behavior for each knockout, and compared the two resulting distributions for 500 each monkey. For Monkey G, eliminating inter-region edges had a significantly greater impact on the correlation between ACE and ACF than removing intra-region edges (d = 1.4348, p = 0.0030), while there were no differences in the impact of inter- versus intra-region edge lesions on the correlations between ACE and ASF or CLE. For Monkey Y, there were no differences in the impact of inter- versus intra-region edges lesions on 505 correlations between ACE and any of the saccade behavioral metrics. In general, we note that differences in the impact of inter- versus intra-region edge lesions on the relationship between control energy and behavior are limited and individual-specific.

The observed behavior-energy correlations exhibited resilience to disruptions in the inferred effective connectivity (See Supplementary Figure 10). In order to successfully 510 disrupt the observed correlations in Monkey G, a minimum of 84% of all edges from its connectivity matrix have to be removed. This minimum threshold increases for Monkey Y, where at least 95% of all edges have to be set to zero in order to significantly disrupt the correlations. These findings suggest that the energetic constraints on neural state transitions relevant for behavior are only partially localized (Figure 6B & Figure 6C), but 515 may be more accurately described as being broadly distributed across the circuit.

Discussion

Learning commonly requires the development of strategies to increase reward in the face of uncertainty⁴⁰. Such strategies can be manifested in sequential behaviors that serve to continuously gather information about the environment³. Yet precisely what rules 520 guide the formation of sequential behaviors remains poorly understood. Although recent work highlights the relevance of distributed cortico-striatal circuitry⁴¹, progress has been hampered by the lack of a formal theory linking activity in such circuitry to habitual (or non-habitual) behavior. Here we address this challenge by employing network control theory to determine the energy requirements of sequences of neural states occurring atop 525 a complex network structure.

Combining behavioral measurements and neural recordings from two female macaque monkeys performing a free-view scanning task over 60–180 sessions^{3,6}, we find that smaller energy requirements are associated with transitions between trials in sessions with a high degree of similarity between complex saccade patterns, and in sessions characterized by an 530

emphasis on the repetition of a small subset of patterns rather than exploration of a more diverse set of distinct patterns. We also find that monkeys tend to rely on scan patterns of intermediate complexity, and that within this limited range, complexity and control energy are inversely related. Together, these findings are consistent with the principle of maximum entropy, as they suggest that the distribution of scan patterns maximizes unpredictability over the feasible set of states defined by energetic and behavioral constraints, favoring low-energy, intermediate-complexity patterns while avoiding the extremes of very simple or very complex patterns. Moreover, we employ a virtual lesioning approach to demonstrate that the derived relationships between control energy and behavior are highly resilient to small, local disruptions in the network, suggesting these observations are associated with 540 the network as a whole rather than a small subset of its nodes.

Earlier studies of these data provide evidence for learning of habitual behavior in the absence of instruction and define neural signals underlying the development of habitual behavior sequences. Saccade patterns were found to become increasingly repetitive and lower in entropy over the course of repeated task trials³, and neurons within the caudate 545 nucleus were found to signal both cost and outcome in the context of habit learning⁶. Our work builds on these previous studies by determining how interactions between regions of the frontal cortex and caudate nucleus give rise to habit learning and highlights individual differences in the spatially distributed nature of neural activity that drives learning. More broadly, our study advances a theoretically principled approach to the 550 study of habit formation, provides empirical support for those theoretical principles, and offers a blueprint for future studies seeking to explain how behavior arises from changing patterns of activity in distributed neural circuitry.

The study of habit learning, like the study of many other cognitive functions, has benefited immensely from lesion studies \$^{42-45}\$ and from focused recordings in single brain 555 regions \$^{6,46-48}\$. Yet, the field has long appreciated that single regions do not act in isolation, but instead form key components of wider circuits relevant for perception \$^{49,50}\$, action \$^{51}\$, and reward \$^{52}\$, among others. With recent concerted funding support \$^{53}\$, many new technologies are now available for large-scale recording of neural ensembles, including methods for high-density multi-region recordings \$^{54,55}\$ and associated novel electrode technologies \$^{56}\$. 560 These advances support a wider goal to gather evermore detailed measurements of activity across the whole brain \$^{57}\$. Here, we capitalize upon such technological advances, and utilize multi-channel, multi-area recordings to better understand the distributed nature of neural circuitry underlying habit formation. The channels span Brodmann areas 8 (frontal eye fields), 9 (dorsolateral and medial prefrontal cortex), 13-14 (insula and 565 ventromedial prefrontal cortex), 24-25 (anterior and subgenual cingulate), and 45-46 (pars triangularis and middle frontal area), allowing us to probe multi-area activity and inter-areal interactions that track habitual behavior.

Our data naturally motivate the question of how circuit activity supports behavior.

This question is certainly not new, and not even specific to neural systems. In fact, the 570 recent rapid expansion of work in artificial neural networks has highlighted the fundamental fact that the architecture of a network is germane to the system's function⁵⁸. Liquid state machines⁵⁹, convolutional neural networks⁶⁰, and Boltzmann machines⁶¹ all perform distinct tasks defined by their architectures. Similarly, in biological neural systems, empirical and computational evidence links the architecture of projections with the nature 575 of memory retrieval⁶², flexible memory encoding⁶³, sequence learning⁶⁴, and visuomotor $transformation^{65}$. Intuition can be drawn from simple small architectures or network motifs⁶⁶ which have markedly distinct computational and control properties⁶⁷. For example, a chain is conducive to sequential processing, whereas a grid is more conducive to parallel processing. Unfortunately, the architecture of multi-area circuits in the primate brain 580 is not quite so simple, thus hampering basic intuitions and straightforward predictions. To address this challenge, we use the mathematical language of network science⁷. The network approach allows us to embrace the distributed nature of neural circuit activity and quantitatively describe the empirically observed architecture, while also formalizing questions regarding how that architecture supports circuit function 12 . 585

Current efforts in computational and systems neuroscience are divided by a focus either on patterns of neural activity or on patterns of neural connectivity. At the small scale, this divide separates studies of the firing rates of neurons from studies of noise correlations^{68,69}. At the large scale, this divide separates studies using general linear models or multivoxel pattern analysis in fMRI^{70,71} from studies using graph theoretical 590 or network approaches¹². A key challenge facing the field is the need to span this divide, both in experimental and in theoretical investigations⁷². Indeed, to take the next step in understanding behavior requires the development of computational models of cognitive processes that conceptually or mathematically combine activity and connectivity¹¹.

Here we summarize firing rate activity across channels as a brain state, and we probe 595 how such states can change given the effective connectivity between channels. The fact that network architecture can constrain the manner in which activation patterns change (and $vice\ versa^{73}$) is supported by empirical evidence in large-scale human imaging⁷⁴, and a long history of computational modeling studies in human and non-human species^{72,75}. Here we inform our modeling choice by noting a particular characteristic of that constraint, 600 which exists in the following form: state x is more likely than state y given network A. Specifically, we acknowledge that neural units that are densely connected are more likely to share the same activity profile than neural units that are sparsely connected, for example due to being located in a distant area. This phenomenon naturally arises in many dynamical systems⁷⁶⁻⁷⁸, and its study has recently been further formalized in 605 the emerging field of graph signal processing^{79,80}, which offers quantitative measures to evaluate the statistical relations between a pattern of activity and an underlying graph.

Beyond positing a probabilistic relationship between activity and connectivity, we

define an energetic relation between them. Our formalization uses the nascent field of network control theory^{18–20}, which develops associated theory, statistical metrics, and 610 computational models for the control of networked systems, and then seeks to validate them empirically. The broad utility of the approach is nicely exemplified in recent efforts that address such disparate questions as how to control the spread of infectious disease in sub-Saharan Africa⁸¹, of current in power grids⁸², or of pathology in Alzheimer's disease⁸³. In the context of neural systems, the theory requires three components: (i) a definition 615 of the system's state, such as population-level activity in large-scale cortical areas²² or cellular activity in microscale circuits²⁵, (ii) a measurement of the connections between system components, such as white matter tracts⁸⁴ or synapses⁸⁵, and (iii) a form for the dynamics of state changes given a network, such as full non-linear forms⁸⁶ or linearization around the current operating point⁸⁷. Here we let the state reflect the firing rate activity 620 across channels, the network reflect effective connectivity between channels, and the dynamics take the form of a linearization around the current operating point.

After formalizing the theory for a given system, one can use longstanding analytical results to estimate the energy required to move the system from one state to another^{88,89}. Our approach assumes that the system is linear. Though this assumption is inconsistent 625 with neural dynamics at the microscale cellular level, which are non-linear, prior work indicates that linear models more effectively approximate macroscale neural dynamics than non-linear models and are more readily interpretable⁹⁰. A linear model is therefore suitable for modeling the population-level neural dynamics represented in our data.

We focus specifically on the problem of identifying the minimum control energy, which 630 is a common subform of the more general problem of identifying the control energy required in the optimal trajectory between state i and state j^{91} . Outside of neuroscience, the approach has proven useful, for example, in increasing energy efficiency in induction machines⁹², enhancing performance of transient manufacturing processes⁹³, and managing energy usage in electric vehicles⁹⁴, among others. In the context of neural systems, the 635 study of such trajectories has been used to address questions of how the brain moves from its resting or spontaneous state to states of task-relevant or evoked activity, how the brain's network architecture determines which sets of states require little energy to reach, and how electrical stimulation induces changes in brain state²². Here, we use the approach to estimate the amount of energy that is theoretically needed to push the circuit from the 640 state reflecting firing rate activity in one trial to the state reflecting firing rate activity in the next trial. By performing the calculation for all pairs of temporally adjacent trials, we are able to examine changes in energy over the course of learning. More importantly, structuring the investigation in this way allows us to determine how such energy relates to pairwise differences in sequential behaviors during habit formation.

In an expansion upon prior work in the application of network control theory to neural systems, we posit that low energy state transitions characterize processes (and their

associated behaviors) that are less cognitively demanding. Informally, the underlying notion harks back across at least two centuries in the history of neuroscience⁹⁵. Formally, we can draw insight from the principle of maximum entropy³⁴: when estimating probability 650 distributions (or transitions in this case), the probabilistic transitions that leave the largest remaining uncertainty in the system (i.e., the maximum entropy) are naturally the most unbiased ones in representing the system. Based on this principle, we can thus posit that transitions between low entropy saccade patterns require greater effort and therefore energy than transitions between high entropy saccade patterns. Note that a high entropy 655 saccade pattern is one that spans many targets in a disordered manner while a low entropy saccade pattern is one that spans few targets in an organized, structured pattern.

Concretely, we operationalize the entropy of a TRSP (not to be confused with the monkeys' cluster label entropy that quantifies the extent to which the monkey selects saccade patterns from trial to trial in an ordered fashion) as its fractal dimension, which we refer to as its complexity. Consistent with our hypothesis, we find that the saccade complexity is negatively correlated with the energy theoretically required to move the neural circuit from the firing rate state of one trial to the firing rate state of the next trial. Broadly, our data join those acquired in other model systems, anatomical locations, and species in providing evidence that maximum entropy models explain key features of 665 neural dynamics $^{30-32}$.

Moving beyond the assessment of a saccade pattern's entropy, we next consider the role of habits in modulating the cognitive demands elicited by a task^{96,97}. We hypothesize that transitioning between the same (or similar) saccade patterns will require less cognitive effort, and therefore less energy, than transitioning between different (or dissimilar) saccade 670 patterns. Consistent with our hypothesis, we find that transitioning between more similar saccades is associated with smaller predicted energy, and that sessions with a larger number of distinct saccade patterns are associated with greater predicted energy. Collectively, these data comprise a formal link between the energetics of neural circuit transitions and sequential behaviors.

675

685

By definition, the theoretically predicted energy is a function of both the neural states and the underlying network of effective connectivity, and therefore reflects contributions from all channels and from all inter-channel relations. Nevertheless, it is still of interest to determine whether some channels, or some inter-channel relations, contribute relatively more or less than others, as such regions (or edges) can be targeted with external 680 stimulation to alter behavioral output and potentially guide clinical practice²². Using a virtual lesioning approach, we found that removal of connections in the caudate nucleus, and connections between BA-8, BA-9/45/46 and BA-13/14, resulted in predicted energies that caused small but significant decreases in magnitude to the correlation with saccade metrics.

Our work builds on prior studies by highlighting the importance of network-level

coordination of cortical and subcortical regions for habit learning behavior. The caudate nucleus, frontal eye fields, and prefrontal cortex have been shown to play distinct roles in learning and saccade behavior. Specifically, the frontal eye fields and other regions of the cortex are involved in saccade target selection⁹⁸. The role of prefrontal cortex is consistent with transcranial magnetic stimulation studies showing its necessity for higher-level sequential behavior⁹⁹ and its involvement in uncertainty driven exploration¹⁰⁰.

The critical role of the caudate nucleus in habit formation is consistent with prior lesion studies^{42–45} and recording studies^{6,46–48}. Neurons within the caudate nucleus have previously been shown—using the same dataset analyzed in the present study—to encode 695 both the cost and benefit of performing a given sequence of behaviors⁶ and their activity is correlated with successful learning of stimulus-outcome associations¹⁰¹. Among the edge type lesions that were found to significantly impact the relationship between control energy and saccade metrics, most (50% for Monkey G and >85% for Monkey Y) involved the caudate nucleus. This finding furthers our understanding of the critical role of the 700 caudate nucleus in learning stimulus-outcome associations and informing the development of habitual behavior.

The caudate nucleus and cortex interact via cortico-striatal loops¹⁰², and the caudate nucleus is thus anatomically positioned to receive input from as well as to provide feedback to cortical regions that guide saccade target selection. Our findings build on those of 705 prior studies by demonstrating that virtual lesioning of connections both within and between regions of the cortex and caudate nucleus reduces correlations of ACE with saccade behavioral metrics. Our subsequent random lesioning results further extend our understanding of the neuroanatomical support for these behaviors by suggesting that the energetic constraints on neural state transitions are broadly distributed across the 710 circuit. Furthermore, given that the majority of network edges needed to be lesioned for the behavior-energy correlations to be impacted, it could also be argued that the network architecture itself might not play as significant of a role in energetically constraining the neural state transitions. Future work should investigate this possibility, and examine whether the spatial scale (i.e., number of nodes) or architecture of the network determines 715 how resilient its behavior-energy relationship is to external perturbations.

Lastly, another feature of our findings that we find perhaps particularly striking is their specificity to the two monkeys. Monkey G performed more dissimilar saccade patterns from trial to trial, consistent with the goal-directed exploration supported by prefrontal connections identified in our lesioning analysis. In contrast, Monkey Y performed more 720 similar saccade patterns from trial to trial during sessions, consistent with lower-level habit formation supported by caudate nucleus identified in our lesioning analysis. While our study is underpowered to formally probe individual differences, it would be particularly interesting to examine how the energy-behavior relations described in this work differ across a larger number of individuals. A fruitful future endeavor would also include 725

investigating how the energy-behavior relationships differ between healthy and diseased individuals.

Several methodological considerations are particularly pertinent to this work, and here we mention the three that are most salient. First, we note that in understanding the manner in which neural units communicate, one might wish to have full knowledge of the 730 structural wiring between those neural units 103,104. Despite recent advances in technology at the cellular scale 105–107, such information is challenging to acquire *in vivo* in large animals, and currently not possible at all in primates. A reasonable alternative is to use the empirical measurements of activity to *infer* the effective relationships between neural units 26,108,109. Here we take precisely this tack, thereby distilling a weighted effective 735 connectivity matrix summarizing the degree to which each channel statistically affects another.

It has been found that effective connectivity is generally shaped by anatomical connectivity^{26,110,111}, and may therefore convey similar information about the network's structure. The use of effective connectivity in our model is also consistent with the notion that both structural connections and functional integration within neural systems contribute to their controllability¹¹². A marked benefit of effective over structural connectivity between large-scale brain areas is that only the former can be used to study temporal variation on the time scale at which learning occurs¹¹³. Nevertheless, there are limitations associated with this approach. Changes in effective connectivity may occur over shorter time scales than changes in structural connectivity, particularly during learning, and the average effective connectivity matrix used to compute minimum control energy in this study may not completely capture the relations between brain regions. The neurons recorded may also change over time due to shifts in electrode positioning during the study, potentially leading to changes in effective connectivity that our approach does not capture.

Finally, of relevance to this methodological consideration, missing or "hidden" nodes could impact the integrity of either structural or effective connectivity measures. Although the results of our sub-graph sampling simulation analysis suggest that increasing the number of nodes in the network does not disrupt the relationship between control energy 755 and behavioral metrics (Supplementary Figure 5), future work including recordings from a larger number of brain regions could experimentally validate the persistence of the energy-behavior relationships studied in this work. Such an examination would be of particular interest in assessing whether the relationship between control energy and saccadic movements depends on the spatial scale of the network (i.e., number of cortical 760 and subcortical brain regions observed). From a graph theoretical standpoint, such work could be used to inform whether properties of a subgraph sample can represent properties of the full graph from which they have been sampled.

A second important consideration pertinent to our work is that we use analytical results

from the study of linear systems⁹¹ to inform our network control theory approach^{19,22}. 765 It is well known that neural dynamics – measured in distinct species and across several imaging modalities – are in fact non-linear 75. Linear models of non-linear systems are most useful in predicting behavior in the vicinity of the system's current operating point²¹, or for explaining coarse time-scale population-average activity¹¹⁴.

Of particular relevance to our results is the recent validation of a tight relationship 770 between control energy and metabolic energy¹¹⁵, where increased minimum control energy was found to be correlated with hypometabolism as measured by FDG-PET. Of equal relevance to our results is the recent validation of the use of linear models for neural data⁹⁰, where linear models outperformed a wide breadth of non-linear models in predicting fMRI and iEEG data with minimal model complexity. Although a direct assessment of the 775 performance of linear and nonlinear models for approximating neural dynamics measured by multi-unit electrode recordings has not has not yet occurred, we would expect the results of Nozari et al. to generalize due to the relevance of the four factors that were found to mask nonlinearities in that study: averaging over space and time, observation noise, and limited data samples. For the study of other sorts of behavior or signals, future 780 work could consider extending our simulations to include appropriate nonlinearities 18.

A third important consideration relevant to our work is the fact that animal behaviors in general – and saccades in particular – are complex and difficult to describe cleanly ^{116,117}. Here we address this difficulty by developing a novel algorithmic approach to the extraction of representative saccade patterns. We specifically chose to represent repetitive, cyclic 785 saccadic movements as 2-D polygons (i.e., TRSPs) drawn on the 3×3 grid of equally sized and spaced dots presented during the task; every saccade was represented as a straight line between two dots on the grid. Given the setup of the task, this previously used approach^{3,6} is able to faithfully capture a variety of different saccadic patterns visited. Broadly, our method capitalizes on a graphical representation of saccades, which in turn 790 allows us to use previously developed tools for the characterization of graphs.

There are limitations associated with this approach that warrant mentioning. First, this approach is based on the assumption that meaningful differences in behavior reflective of habit learning are associated with changes from one trial to the next; however, changes in behavior over the course of a trial are not represented. Second, saccade metrics are 795 designed to be rotationally invariant; however, it is known that monkeys possess innate preferences for saccades in one direction. In future work, it would be of interest to assess whether the energetic cost associated with performing a saccade in a particular direction reflects this side bias—in other words, is it less costly to perform a saccade in the preferred versus the non-preferred direction?

Finally, saccade complexity could be influenced by the arrangement of targets in the task, and this possible influence could limit the generalizability of the results. For instance, if targets were arranged in a circle instead of a grid, an ordered pattern of saccades that is

800

low in complexity might be more effective than a complex pattern. If targets were instead arranged at random, a more complex pattern might be more energetically favorable. 805 Of course, other representations—and further analyses—of saccadic trajectories can be employed, such as embedding the saccadic waveforms into higher-dimensional spaces. Our effort follows a growing literature using network models to parsimoniously represent and study animal behavior 118,119. In the future, eye-tracking task setups capturing saccadic movements across a larger number of data points across the grid could be employed.

Systematically canvassing uncertain environments for reward induces habitual behaviors and engages distributed neural circuits. Here we offer a formal theory based on the principles of network control to account for how pairwise differences in sequential behaviors during habit formation can be explained by the energetic requirements of the accompanying neural state transitions. In doing so, the study frames the concept of cognitive computations within a formal theory of network energetics. Our findings further support the notion that the principle of maximum entropy could be a useful explanatory principle of behavior. While outside the scope of this study, many relevant questions remain unasked. Future work could usefully expand upon our observations by increasing the number of recorded regions or altering the task to include different sorts of environmental uncertainties. 220 Incorporation of additional computational capabilities into the theory, and exercising agent-based simulations to determine optimal cost functions and associated learning rules for artificial neural systems placed in similar environments could also be used to expand upon this work.

Methods 825

The data consist of behavioral measurements and neural recordings from two adult female monkeys (Maccaca mulatta, 5.9kg each): Monkey G and Monkey Y. All procedures were performed as approved by the Massachusetts Institute of Technology's Committee on Animal Care. Full descriptions are provided in earlier publications on this dataset^{3,6}, and here we briefly summarize.

830

Both monkeys were individually monitored, and data was recorded while the monkeys performed a free-viewing scan task. The task was performed across multiple days (sessions) with each session consisting of multiple back-to-back trials. Eye movements were recorded utilizing an infrared tracking system and converted into a sequence of saccades, or rapid eye movements from one point to another. All measurements of neural activity were 835 obtained from individual chronically implanted electrode arrays recording bilaterally from various points in the caudate nucleus, frontal eye fields, and prefrontal cortex.

Recording Technology

Prior to neural recordings, a head fixation post and recording chamber were placed in separate surgeries. All surgical procedures were performed under sterile conditions on 840 deeply anesthetized monkeys placed in a standard stereotaxic apparatus. Each recording chamber was centered mediolaterally on the midline of the brain (with 20 mm on either side) and at approximately 22 mm (monkey G) or 30 mm (monkey Y) anterior to the interaural line.

The plastic recording chamber accommodated a 30 \times 40 mm grid with holes spaced at 1 mm center to center. These holes accommodated custom-built screw microdrives (Specialty Machining) that could each carry three, six, or nine independently movable electrodes (1–2 M Ω at 1 kHz, 110-130 mm long, 125 μ m shank, 3 μ m diameter tip; Frederick Haer). The microdrives could be configured to space electrodes as close as 1 mm apart and to record simultaneously from many brain regions, and their placements could be reconfigured for each chronic implant. Before the implantation of the chronic electrodes, electrophysiological mapping by the use of microstimulation (trains of 24-64 250 μ s wide biphasic pulses, 333 Hz, 10-150 μ A) was completed to determine the location of several key landmarks such as the FEF, primary motor cortex, and the depth of the dorsal surface of the CN.

Data from monkey G is from one chronic implant containing 72 independently movable electrodes targeting the CN, FEF, and PFC bilaterally. It was in place for 140 days. Both of the chronic implants (166 and 366 days, respectively) in monkey Y contained 96 electrodes and also bilaterally targeted the CN, FEF, and PFC.

The recording of all data (behavioral and neural) began on the first day of training after electrodes had been implanted. Eye position was monitored by an infrared eye tracking system (500 Hz; SR Research Ltd.). Custom behavioral control software was designed in Delphi III. All signals were recorded with a Cheetah Data Acquisition system (Neuralynx, Inc.). Spike waveforms were digitized at 32 kHz (filtered 600-6,000 Hz). Local field potentials were filtered at 1-475 Hz, and eye movements were recorded at 2 kHz.

Task Structure

The task begins when a grid of small gray circles is presented on a screen in front of the monkey, whose head is fixed in place. After a variable period of time, the inner gray circles of the grid are replaced with a 2×2 grid or a 3×3 grid of larger green dots (Targets On). The monkey's gaze may not leave the space defined by the perimeter of the green dots or 870 the trial will be marked as unsuccessful and the screen will revert back to a grid of only gray dots. After a variable time, one of the green targets is baited (Target Baited) such that if the monkey's gaze falls on to the baited target, the trial is rewarded. The monkeys were not given information about when the target was baited or which target was baited.

At this point in the task, if the monkey's gaze crossed into or over the bait target, the grid of green dots was replaced by the original gray dots (*Targets Off*). After a variable time, the monkey was presented with a short reward to indicate success; acknowledging their preferences, juice was offered to Monkey G, and an alternative reward mixture was offered to Monkey Y.

880

900

Data Quality Assurance and Cleaning

Due to the inherent complexity of the task and behavioral responses thereto, it is critical to apply data quality standards that ensure statistical analyses are appropriate and well-powered. Accordingly, all analysis involved in inferring effective connectivity was limited to task trials where the monkeys were presented with the 3×3 grid version of the free-scanning task. Early sessions in which the 3×3 grid were not present were excluded session the analyses. Furthermore, the number of available channels, defined as those with non-zero signal, varied across sessions. The 60 recorded sessions for Monkey G contained anywhere from 16 to 38 channels (with an average of 23) from a total of 72 unique channels. The 180 recorded sessions for Monkey Y contained anywhere from 3 to 23 channels (with an average of 11 channels) from a total of 96 unique channels.

To ensure adequate sampling, all analysis performed on Monkey Y was limited to sessions containing 8 or more channels. These criteria resulted in 18,298 available trials for Monkey G and 157,729 for Monkey Y. Analytical steps focused on defining the relationship between task behavior and control energy dynamics were limited to only 3×3 grid task trials that were rewarded and exhibited a looping saccade sequence, which is defined as sequence that starts and ends at the same grid target. A total of 9,702 ($\sim53\%$) task trials were used for Monkey G and 80,664 ($\sim51\%$) for Monkey Y. In this particular task, a looping saccade sequence in which all targets were visited once before returning to the starting node is considered optimal³.

Classification of Saccade Sequences

Measurements of monkey eye-movements during the free-scanning task comprise a list of saccades performed in the scanning window of a given trial. Each saccade is represented as a vector of two numbers, which denote the start and end grid targets of the saccade. The entire sequence of saccades performed during a given trial can be written as an $m \times 2$ matrix, SL. Each row in SL is a single saccade, with the first and second column 905 representing the start and end targets, respectively. This representation can be thought of as a list of directed connections between points. It is then possible to convert a trial specific sequence of saccades into a directed and weighted graph, which we will refer to as the saccade network.

In graph theory⁷, a generic network is made up of N nodes that are connected pairwise 910 by E edges. Here, a saccade network consists of nine nodes (N = 9), one for each grid target, and edges defined by the saccade sequence. Specifically, an edge between two nodes in a saccade network exists if a saccade was performed between those two targets. The weight of the edge is given by the number of times that specific saccade was performed. Therefore, the saccade network can be written as the directed and weighted $N \times N$ 915 adjacency matrix, \mathbf{S} , whose element S_{ij} denotes the weight of the edge between node i and node j. Edges with zero weight signify no connection.

We seek to identify unique saccade patterns across trials, which will in turn allow us to investigate how performance strategies might evolve throughout the task³. We refer to the unique saccade pattern performed during a given trial as the trial representative 920 saccade pattern (TRSP). To identify the TRSP, we utilize the saccade network of a given trial and identify all the cycles in the network. In graph theory, a cycle is defined as a series of edges that allows for a node to be reachable from itself. Therefore, a cycle in the saccade network is a loop that starts and ends on the same target. This cycle can be represented as a binary cycle matrix, \mathbf{L} , of size $N \times N$; a given element of \mathbf{L} is set to 925 one if the corresponding edge is a part of the cycle. We take the dot product of the cycle matrix \mathbf{L} and the saccade network \mathbf{S} , and refer to the resulting matrix as \mathbf{L}' . For a given saccade network, multiple cycles can exist, and therefore also multiple \mathbf{L}' s. We define the TRSP to be the cycle with the greatest element-wise sum of all weights in its \mathbf{L}' , which intuitively is the cycle composed of the most common point-to-point saccades.

To ensure that the TRSP was not merely an outlier cyclic path performed by the monkey, we calculated the sum of edge weights corresponding to each cyclic saccadic path and assessed how much larger the TRSP-derived sum was compared to that of the remaining cyclic paths visited. For Monkey G, the averaged (across all trials and sessions) TRSP was 1 standard deviation away from the mean of weighted edge sums of all other cyclic paths (min-max standard deviations range: [0.45, 2.78]); for Monkey Y, the averaged TRSP was 1.01 standard deviation away from the mean of weighted edge sums of all other cyclic paths (min-max standard deviations range: [0.38, 3.06]). These results highlight two points: (i) the TRSP across each trial was not an outlier cyclic path performed by the monkey (when defining an outlier as a data point that is 4 standard deviations away from the mean), and (ii) the TRSP patterns of both monkeys were very similar to each other (as shown by the aforementioned, highly similar min, max, and mean ranges). For an intuitive graphical depiction of this process, see **Supplementary Figure** 1.

To characterize the similarity between trial saccade sequences, we first considered the 945 challenge of comparing two saccade patterns. Many statistics exist for comparing graphs, but it is often unclear which is most appropriate in a given context¹²⁰. To circumvent this issue, it is useful to consider the cyclic path between nodes in a single TRSP to be a 2-D

polygon drawn on the 3×3 grid of equally sized and spaced circles presented during the task. Every saccade that is a part of the pattern is represented as a straight line between 950 two centers of circles on the grid. Each line can then be discretized into small segments, allowing it to be summarized as the set of 100 (x,y) coordinates of segment centers. In other words, each saccade pattern can be summarized by the set of n points, P:

$$P = \{(\mathbf{x}_i, \mathbf{y}_i) \mid (\mathbf{x}_i, \mathbf{y}_i) \in \mathbb{R}^2\}, \text{ for } i = 1, \dots n.$$
 (1)

which finely samples the lines composing the saccade polygon.

While a set of points is a simpler representation than a graph, it remains difficult to 955 compare these point sets in a manner that accounts for the original geometry. To address this difficulty, we first calculate the centroid of the saccade polygon, C, and then we calculate the Euclidean distance between C and every point in P:

$$D_{i} = \sqrt{(P(\mathbf{x}_{i}) - C(\mathbf{x}_{i}))^{2} + (P(\mathbf{y}_{i}) - C(\mathbf{y}_{i}))^{2}}$$
(2)

Indeed, we found the centroid measure to be robust to noise (Supplementary Analysis 1) and to exhibit a 1:1 relationship with its corresponding TRSP (Supplementary 960 Analysis 2). Then D is a 1-D saccade waveform that parsimoniously represents the saccade polygon while maintaining geometric information. This 1D interpolation represents a standard approach to describing polygons that yields a continuous function. To ensure comparability across polygons and that all saccade waveforms are being compared to the same number of data points, we interpolate each D to I = 600 points. Using this approach, 965 we could include a large number of data points that would generate a continuous function and thereby accurately capture differences across saccadic waveforms. To assess the robustness of our results to other choices of I, we also used a range of different Is (range: 400 to 700) and re-calculated the variables of interest: average similarity factor, average complexity factor, and cluster label entropy, described below. The recomputed variables were statistically highly similar (Pearson's $\rho > 0.7$; $p < 10^{-6}$, across all comparisons) to the ones obtained when using I = 600 points, indicating that our choice was a representative one.

The fact that the saccade waveform can be thought of as a time-series representation of a saccade pattern informs our measure of similarity. Importantly, we wish our measure 975 to be invariant to rotation and reflection, such that two polygons rotated by 90 degrees from one another or two polygons which are direct mirror images of each other are correctly determined to be the same. Therefore, rather than simply calculating the Euclidean distance between two saccade waveforms, we instead calculated the Euclidean distances between one saccade waveform and a series of circularly shifted versions of the 980 second saccade waveform. A circular shift is a mathematical operation where a vector is

rearranged such that the last element is moved to the first position and all other elements are shifted forward by one. By performing this operation l times, it is possible to shift the last l values to the front of the vector and all other values forward by l positions.

Accordingly, we create a set of circularly shifted saccade waveforms that represent rotations of the original saccade sequence by different angles as well as rotations of the mirror image of the original saccade sequence. The mirror image of the saccade sequence can be represented by flipping the saccade waveform from left to right (see Supplementary Figure 7). We write the angle of rotation as $\alpha = 360(\frac{l}{l})$. For each pair of saccade sequences, a two-step approach is used to quantify their dissimilarity. First, for each pair we calculated the Euclidean distances between one saccade waveform and the circular shifts of a second saccade waveform (including its mirror image representation) in intervals of $\alpha = 6$ degrees such that $l \approx 10$. From this set of calculations we identify the circular shift which resulted in the smallest Euclidean distance and denote its index as i_{min} . Next, we repeated the above process but now performed shifts of size l = 1 such 99 that $\alpha \approx 0.58$. These fine-grained secondary calculations included only circular shifts between $i_{min} - 1$ and $i_{min} + 1$. The dissimilarity factor (DF) between the two saccades was taken to be the minimum of the calculated distances in the second step; saccades with large distances between them are more dissimilar.

To summarize the saccade pattern similarity between two adjacent trials within a task 1000 session, we defined the SF. For each session s containing T_s trials, the saccade dissimilarity was calculated between saccade patterns from pairs of consecutive trials as described in the previous section. Each value was then converted into a measure of similarity as follows: $SF = 1 - \frac{DF}{DF_{max}}$, where DF_{max} is the maximum DF observed out of all trials from both monkeys. For each session the ASF was then given by the average of all SFs calculated 1005 for that session. See **Supplementary Figure 8a** for the ASF as a function of session for both monkeys.

To characterize the complexity of each saccade pattern, we defined the CF. We operationalized the notion of complexity as the fractal dimension 121,122 , which has proven useful in the study of many other biological 123,124 and network systems 125 . For each TRSP, 1010 we first constructed a binary image of its polygon representation, where the background was black and the saccade pattern outline was white. We then applied the box-counting method to this image to compute the fractal dimension 126 . Due to the nature of this method, two identical patterns rotated by 90 degrees from one another would result in different fractal dimension values. Therefore, the final fractal dimension value for each trial 1015 pattern was taken to be the minimum calculated from the set of all possible rotations of the pattern and its mirror image at intervals of 90 degrees. For each session, s, containing T_s trials, the ACF was given by the average fractal dimension of all trial representative saccade patterns in that session. See **Supplementary Figure 8b** for the ACF as a function of session for both monkeys.

To quantify the extent to which the monkey selects saccade patterns from trial to trial in an ordered fashion, we defined the CLE metric. More precisely, our goal was to determine whether the monkey was randomly performing various patterns or selectively repeating only a few unique ones. We began by using the MATLAB function linkage() to perform agglomerative clustering on the unique saccade waveforms from all the trials of 1025 an individual monkey¹²⁷. The algorithm outputs a hierarchical, binary cluster tree, also known as a dendrogram, based on an input of a $T \times T$ distance matrix, where the ij-th element gives the DF between the saccade pattern of trial i and the saccade pattern of trial j. The height of a link between two objects in the dendrogram directly denotes the distance between those two objects in the data.

It is important to note that the dendrogram itself does not indicate the optimal number of clusters that the data should be split into; rather, it demonstrates the order in which objects should be clustered. However, there is a way to identify the natural divisions of the data into distinct clusters using the derived cluster tree. The inconsistency coefficient metric is used to compare the height of a link in a cluster tree to heights of all the other 1035 links underneath it in the tree. If the difference is dramatic, it signifies that that newly formed group consists of linking two highly distinct objects. Imposing a threshold on the inconsistency coefficient during clustering captures more natural divisions in the data rather than arbitrarily setting a maximum number of possible clusters.

Accordingly, using the MATLAB function *cluster()* we constructed clusters from 1040 the hierarchical cluster tree using a range of inconsistency coefficient values (0.1-1.5 in intervals of 0.05) as a threshold criterion, and then calculated the average within cluster sum-of-squares. Using the elbow-method and the calculated within cluster sum-of-squares, we selected an inconsistency coefficient of 0.95 to be the optimal threshold criterion for clustering. This choice resulted in a total of 136 clusters being identified for Monkey G 1045 (out of a total of 276 distinct paths) and 346 for Monkey Y (out of a total of 801 distinct paths). See **Supplementary Figures 2 and 3** for a detailed listing of cluster patterns of both monkeys.

After coarse-graining the data by identifying saccade clusters across trials and sessions, we next turned to assessing whether the monkey transitioned between saccades of the 1050 same cluster or of different clusters, and to what degree. We began by identifying the representative saccade sequence of each discovered cluster by finding the TRSP that had the minimum sum of the DF when compared to all other within-cluster patterns. For each session, we then calculated the *CLE* as Shannon's information entropy of a given session's vector of trial cluster labels. See **Supplementary Figure 8c** for the saccade 1055 cluster entropy as a function of session for both monkeys.

Channel Firing Rates

Information about neuronal activity was not available for all channels during each session; some channels, which we refer to as non-viable channels, showed no activity across all task trials. All non-viable channels were discarded prior to data analysis. Monkey G contained 1060 a total of 59 viable channels and Monkey Y contained a total of 64 viable channels. On average, a given free-scanning task session contained 23 active channels for Monkey G and 11 active channels for Monkey Y. While biologically expected, this variation in channel availability across sessions can adversely affect estimates of effective connectivity (see next section). For example, if we were to compute the effective connectivity from the activity 1065 of all channels across all trials at the same time, we could obtain spurious results due to the incomplete sampling across trials and time.

To mitigate potential biases due to variable channel availability, we estimate the effective connectivity in each session separately. Every session contains N_{CH} channels from which a signal is available. The signal from each channel is in the form of a spike 1070 train, or a vector of ones signifying neuronal activation, and the time at which each activation occurred. All spikes from the full duration of a trial were used when inferring effective connectivity. For analysis concerned with identifying the relationship between behavior and control energy, we focused solely on spikes that occurred after the task grid was presented to the monkeys $(t_{targets\ on})$ and before the task grid disappeared signifying 1075 success $(t_{targets\ of\ f})$. This window of time is referred to as the scanning period (t_{sp}) .

The firing rate r of a single channel is given by the number of spikes per second. Calculation of the fire rate of all channels during an individual trial then results in a $1 \times N_{CH}$ vector that represents the activation state of the channel network during that trial. We will refer to this column vector as the neural state x_t :

$$x_t = \begin{bmatrix} r_1 \\ r_2 \\ \vdots \\ r_{N_{CH}} \end{bmatrix}, \text{ where } t = 1, \dots, T_s$$
(3)

State vectors x_t are calculated for each trial, across all sessions, and for each monkey.

Inferring Effective Connectivity

Effective connectivity provides information that differs from both functional connectivity and structural connectivity²⁶. For nearly three decades, effective connectivity has been "understood as the experiment and time-dependent, simplest possible circuit diagram 1085 that would replicate the observed timing relationships between the recorded neurons" 128. Effective connectivity moves beyond the purely correlational nature of canonical functional

connectivity and provides a means of statistically inferring activity flow across brain regions²⁶. Prior studies from our group and others have previously used effective connectivity in combination with network control theory to identify neural correlates of 1090 brain-computer interface learning¹²⁹ and points of intervention for seizure suppression¹¹², highlighting the feasibility and utility of this approach. In addition, it is important to note that the control of functional connectivity networks necessitates the use of different methods than the control of structural or effective networks¹³⁰.

The pattern of effective connectivity among many units can be usefully represented as 1095 a network, composed of nodes (neural units) and edges (effective connections) derived from node activity. Here, we construct such a network for the set of electrode channels used to record neuronal activity during trials of the free-scanning task. We chose transfer entropy as the method to estimate effective connectivity³⁵, although we acknowledge that other methods exist and could similarly prove useful in the study of habit learning. 1100 Transfer entropy, while unable to infer causal influence between time-series, represents a closer approximation to this goal compared to purely associative methods like Pearson's or Spearman's correlation, which are commonly employed for defining functional connectivity.

Mathematically, the (Shannon) transfer entropy was defined as follows:

$$TE_{Y\to X} = \sum_{i,j} p(i_{t+1}, i_t^{(k)}, j_t^{(l)}) \cdot log(\frac{p(i_{t+1}|i_t^{(k)}, j_t^{(l)})}{p(i_{t+1}|i_t^{(k)})})$$
(4)

where i_t denotes the status of signal time-series X at time t and reflects the average 1105 firing rate associated with a given trial; j_t denotes the status of signal time-series Y at time t; $i_t^{(k)} = (i_t, ..., i_{t-k+1})$ and $j_t^{(l)} = (j_t, ..., j_{t-l+1})$ with k and l denoting the order of the transfer entropy and representing the past spiking history of the signals X and Y, respectively; p denotes probability; and the vertical bar denotes conditional probability. Overall, $TE_{Y\to X}$ quantifies the information flow from signal time-series Y to X, and is 1110 based on the assumption that a time-series Y can better predict the behavior of signal time-series X, if the combined past spiking histories of Y and X are more informative in predicting the future spiking history of time-series X than the past history of X alone^{35,131}.

For each session, we computed the transfer entropy between all pairs of viable-channels from the set of z-scored state vectors x_t of size $1 \times N_{CH}$ to obtain an $N_{CH} \times N_{CH}$ directed, 1115 asymmetrical effective connectivity matrix whose diagonal elements are set to zero. All calculations of transfer entropy were performed using the $calc_te()$ function from the RTransferEntropy package in R.

Rather than utilizing a pre-defined temporal window when estimating transfer entropy, we calculated the overall transfer entropy for each session. For completeness, we gathered 1120 all session effective connectivity matrices into the 3-D matrix \mathbf{M} whose element $M_{k,i,j}$ represents the effective connectivity between channels i and j, derived from the k^{th} session. From the individual session effective connectivity matrices, we calculated the overall

effective connectivity matrix, \mathcal{M} , whose element $\mathcal{M}_{i,j}$ is given by the average of the set of the non-zero connection strengths between channels i and j derived from only the 1125 sessions in which both channels were available. Accordingly, \mathcal{M} is a square directed and asymmetrical matrix of size $N_{TC} \times N_{TC}$, where N_{TC} is the total amount of available channels across all sessions for an individual monkey.

Lastly, to ensure that the generated effective connectivity matrices are specific to the monkeys' functional patterns of activation rather than noise, we compared the nodal 1130 degree distribution of our observed transfer entropy-derived effective connectivity matrix to the nodal degree distribution of a randomly generated set of effective connectivity matrices. Each one of these null connectivity matrices was generated by (i) randomly shuffling the average trial-based firing rate patterns corresponding to each channel (n = 1000 permutations), across channels, (ii) calculating the new transfer entropy based on 1135 these random assignments, and (iii) generating null effective connectivity matrices using these newly-derived transfer entropies. In both monkeys, the nodal degree distribution corresponding to their observed effective connectivity matrix was significantly higher than the nodal degree distribution corresponding to the null matrices (two-sample Kolmogorov-Smirnov test – Monkey G: $ks_{stat} = 0.3051$, p = 0.0062; Monkey Y: $ks_{stat} = 1140$ 0.5, $p = 1.01 \times 10^{-7}$).

Network Control Theory

To build an intuition for how we use network control theory to probe relations between neural circuit activity and behavior, we begin with a few preliminaries. We consider a non-linear dynamical system and linearize those dynamics about the system's current 1145 operating point⁹¹. The dynamics of the resultant linear time invariant (LTI) system can be written as:

$$\dot{x} = \mathbf{A}x(t) + \mathbf{B}u(t) \tag{5}$$

where N is the number of nodes, **A** is the $N \times N$ adjacency matrix,

 $x(t) = [x_1(t), x_2(t), \dots, x_N(t)]$ is the state of all network nodes at time t, $u(t) = [u_1(t), u_2(t), \dots u_K(t)]$ gives the external control input for K number of *driver nodes* 1150 which receive external input in order to drive the state change of the network. In this work, all network nodes are set to be driver nodes (K = N) and as such \mathbf{B} is the $N \times N$ identity matrix.

The minimum control energy is defined to be the minimum amount of energy that a controller requires to drive an LTI system from some initial state to a target final state 1155 in a specified amount of time⁹¹. If there exists an input vector u(t) that can move the defined network from its initial state, x_o , to a state x_f in time t_f , the energy expenditure is given by $E(t_f) = \int_0^{t_f} \|u(\tau)\|^2 d\tau$. Practically, we can calculate the minimum control

energy to reach the target network state (x_f) from an initial state (x_o) as

$$E_{\min}(t_f) = \left(e^{\mathbf{A}t_f}x_o - x_f\right)\mathbf{W}_c^{-1}(t_f)\left(e^{\mathbf{A}t_f}x_o - x_f\right)$$
(6)

where t_f is the time horizon and $\mathbf{W}_c(t_f)$ is the controllability Gramian,

$$\mathbf{W}_{c}\left(t_{f}\right) = \int_{0}^{t_{f}} e^{\mathbf{A}\tau} B B^{\mathsf{T}} e^{\mathbf{A}^{\mathsf{T}}\tau} d\tau \tag{7}$$

for the system. The numerical method used to solve the integral is MATLAB's native numerical "integral" command, and the time horizon is set to a value of 1 (units: dt) for all calculations in this analysis, as previously reported ¹³². We provide references and a discussion on the pros and cons of this method in the Discussion.

Here we use this framework to compute the ACE required to move the neural circuit 1165 from firing rate state x_t to firing rate state x_{t+1} given the effective connectivity $\mathbf{A}_s = \mathcal{M}_{i,j}$ for all channels in that session. Note that x_t and x_{t+1} are the firing rate states of two consecutive trials within a given session. Thus, we obtain an E_{min} value for every consecutive trial pair. The ACE metric is then the average of E_{min} across all state transitions in that session.

Control Energy & Saccade Characteristics

We calculated Pearson correlation coefficients between the three saccade characteristic metrics (SF, CF, CLE) and the ACE. To control for variability in the number of recorded channels (NCH) across sessions, we regressed each variable of interest on NCH using a linear model. We then computed correlations between the resulting residuals, thereby 1175 assessing the relationship between variables independent of NCH. To ensure that all correlations were specific to the control energy dynamics derived from the inferred overall effective connectivity matrix, \mathcal{M} , we permuted that vector of ACE (number of elements = number of sessions considered for each monkey) 1000 times and calculated the Pearson correlation between the permuted ACE vector and the original saccade metric vector 1180 (SF, CF, CLE), for each permutation, to generate a null distribution of correlation coefficients. A one-tailed test was then used to determine the significance of the Pearson correlation coefficients calculated with the original ACE dynamics against their respective null distributions, at a significance level of $\alpha = 0.05$.

We ran a simulation in order to demonstrate that directional tuning alone does not 1185 explain our reported results. Instead of using each Monkey's actual firing rates obtained across each session, channel and trial, to generate its empirical effective connectivity matrix and ACE, we generated a "null matrix" of firing rates using only the monkeys' saccadic behavior. This null matrix was then used to re-compute the monkeys' simulated effective connectivity matrices and corresponding average control energies. The steps we 1190

took to accomplish this computation were:

For each monkey and for each session:

- 1. We first created an array that contained all possible saccadic angles ranging from 0 to 360 degrees that could be taken when traversing across the 9 grid points.
- 2. We then created a new matrix $C \times T$, where C corresponded to the number of 1195 simulated cells (set equal to the number of channels used for that Monkey) and T to the number of trials.
- 3. For each simulated cell, we randomly selected one of the angles reported in step (1) as the cell's preferred direction (i.e., direction tuning). For that angle, we designated an arbitrary firing rate as the cell's maximum firing rate. The maximum firing rate was 1200 represented as the peak of a Gaussian distribution in which distance from the center along the x axis reflected the closeness of each angle to the preferred direction 133 .
- 4. Using this mapping between saccadic angles and firing rates, we computed the simulated cell's average firing rate for each trial, using the Monkey's actual saccades. Thus, for instance, if the Monkey had performed 10 saccadic movements during Trial 1205 1, we extracted the corresponding cell-specific simulated firing rate for each of the 10 saccadic movements using the mapping described in step (3), and then averaged across all 10 firing rates to obtain the average firing rate of cell C during trial T.
- 5. The null matrix $C \times T$ was then used to recompute the Monkey's simulated effective connectivity matrix and corresponding ACE, as reported in the manuscript.
- 6. Lastly, we repeated all main analyses reported in the text using the Monkey's simulated ACE.

The results corresponding to the aforementioned simulation are reported in the "Simulation Analysis" section of the Results.

Network Region Lesion Analysis

For both monkeys, electrode channels recorded bilaterally from regions of the caudate nucleus, frontal eye fields, and prefrontal cortex. In order to examine the extent to which specific nodes or edges contribute to the inferred overall effective connectivity matrix, we performed a virtual lesion analysis. Here, a lesion is operationalized by setting specific elements $\mathcal{M}_{i,j}$ of the effective connectivity matrix to zero, thereby effectively eliminating 1220 the connection between the i^{th} and j^{th} nodes. Each monkey had a unique set of regions, $R = \{R_1, R_2, \ldots, R_N\}$, from which the N_{TC} channels were recording such that each channel was assigned only one region across the entire duration of the task.

1215

For each monkey, we performed two types of lesions. First, we lesioned all the edges between any two regions, R_i and R_j , and we refer to this method as the *inter-region edge* 1225 knockout. Second, we lesioned all edges belonging to the same region, and we refer to this method as the *intra-region edge* knockout. Each lesion results in a knockout effective

connectivity matrix which we denote as \mathcal{M}^{KO} . Therefore, if performing an inter-region edge knockout between the caudate nucleus (R_1) and Brodmann Area 8 (R_2) then \mathcal{M}^{KO} would be the same as the original effective connectivity matrix, \mathcal{M} , except that all 1230 elements that represent connections between R_1 and R_2 are set to zero. In the same way, if performing an intra-region edge knockout lesion of the caudate nucleus then \mathcal{M}^{KO} would be the same as \mathcal{M} but have all elements that represent connections of caudate nucleus nodes to other caudate nucleus nodes set to zero.

To determine the relevance of a connection for an energy-behavior correlation, we used 1235 two criteria. The first criterion was that the lesion resulted in a correlation value that was not significantly different (p > 0.05) from that obtained using the original permutation null model (random permutations of the original ACE vector values). The obtained p-value is referred to as $p_{general}$ (see Supplementary Figure 9b and 9d). To assess this criterion, we calculate the knockout ACE metric, ACE^{KO} , for each lesion and use it to recompute 1240 the Pearson correlation values between ACE^{KO} and the average saccade metrics. We test the significance of each knockout correlation value using a one-tailed test against the null distribution derived from calculations involving the original permutation null model. A knockout correlation that fails to prove significant from the above one-tailed test signifies that the inter- (or intra-) region edges knocked out are important to the inferred effective 1245 connectivity matrix and its relationship to task behavior.

The second criterion for determining the relevance of a connection for an energy-behavior correlation was that the lesion-induced disruption of the observed correlation was specific to the lesion chosen, and not expected by lesioning the same number of randomly chosen edges. To assess this criterion, every knockout correlation value is compared to the original 1250 correlation value by calculating the absolute value of the difference between them, resulting in a correlation difference metric for each lesion. This metric quantifies how strongly the removal of the targeted edges alters the energy-behavior relationship, allowing us to determine whether specific connections are particularly influential in maintaining the observed correlation.

To ensure that the difference in correlations is truly related to the lesion-specific edges, the results were tested using a null model. The null hypothesis states that, for a lesion consisting of n specific edges $E^{KO} = \{e_1, e_2, \ldots, e_n\}$, the resulting correlation difference value is no different from the correlation difference value derived from knocking out n randomly selected edges, $E^{null} = \{e_i \mid e_i \notin E^{KO}\}$. For every lesion, a null distribution of 1260 1000 correlation values was created by randomly knocking out the same number of edges as the original lesion, ensuring that no edge overlapped with those in E^{KO} . All values were tested against their respective null distributions using a one-tailed test with significance level $\alpha = 0.05$. The obtained p-value is referred to as p_{lesion} (see Supplementary Figure 9c and 9e). Gray boxes shown in (Figure 6B-C) indicate edges which, when 1265 lesioned, did not result in a significant change in behavior-energy correlation compared to

the null distribution derived from randomly lesioning edges.

Due to the small magnitude changes in behavior-energy correlations caused by inter-/intra-region virtual lesioning, we next sought to quantify the number of edge lesions that are required to completely disrupt an observed behavior-energy correlation. 1270 Accordingly, for each monkey the resilience of each behavior-control correlation was tested by performing increasingly large lesions and re-calculating the correlation values. The analysis started with 1-edge lesions and ended with lesions involving up to 95% of all available edges. Each lesion was performed 100 times with random edges and the average changes in behavior-energy correlation are shown in **Supplementary Figure 10** for 1275 Monkey G and Monkey Y.

Data Availability

The data that support the findings of this study are available from the corresponding authors upon reasonable request.

Code Availability

1280

Publicly available MATLAB code for implementing the analyses described in the manuscript can be found here: https://github.com/kpszym/SaccadePatternExtraction.git.

Acknowledgments

We thank Eli J. Cornblath, Pragya Srivastava, Christopher W. Lynn, Harang Ju, Sophia David, Jennifer A. Stiso, William Qian, and David M. Lydon-Staley for helpful comments 1285 on an earlier version of this manuscript. The work was primarily supported by an ARO MURI awarded to Bassett & Graybiel (Grafton-W911NF-16-1-0474). The work was further supported by the John D. and Catherine T. MacArthur Foundation, the Alfred P. Sloan Foundation, the ISI Foundation, the Paul Allen Foundation, the Army Research Laboratory (W911NF-10-2-0022), the Army Research Office (W911NF-21-1-0328 1290 to AMG), the National Institute of Mental Health (2-R01-DC-009209-11, R01-MH112847, R01-MH107235, R21-MH-106799, R21MH125010 and R01MH131615), the National Institute of Child Health and Human Development (1R01HD086888-01), National Institute of Neurological Disorders and Stroke (R01 NS099348, R01-NS025529), the National Eye Institute (R01-EY012848), the National Institutes of Health Ruth L. Kirschstein 1295 National Research Service Award (T32-EB020087, F32-AA030475), an NSF CAREER Award (BCS-2143656 to TMD), the National Science Foundation (NSF PHY-1554488, BCS-1631550, and IIS-1926757), and the Cornell Bethe/KIC/Wilkins postdoctoral fellowship,

the Cornell Neurotech Mong Family Foundation postdoctoral fellowship, and the Eric and Wendy Schmidt AI in Science postdoctoral fellowship to JZK. The content is solely the 1300 responsibility of the authors and does not necessarily represent the official views of any of the funding agencies.

Author Contributions

D.S.B, T.M.D. and A.M.G. conceived of the study; T.M.D. and A.M.G. contributed data; J.K.B., P.F., K.S., J.Z.K. and F.P. carried out all analyses and interpreted the results; 1305 J.K.B., P.F., K.S., T.M.D. and D.S.B wrote the manuscript; all authors reviewed and edited the manuscript.

Competing Interests

The authors declare no competing interests.

Citation Diversity Statement

1310

Recent work in several fields of science has identified a bias in citation practices such that papers from women and other minorities are under-cited relative to the number of such papers in the field ^{134–138}. Here we sought to proactively consider choosing references that reflect the diversity of the field in thought, form of contribution, gender, and other factors. We obtained predicted gender of the first and last author of each reference by ¹³¹⁵ using databases that store the probability of a name being carried by a woman ^{138,139}. By this measure (and excluding self-citations to the first and last authors of our current paper), our references contain 10.6% woman(first)/woman(last), 5.8% man/woman, 19.2% woman/man, 57.7% man/man, and 6.73% unknown categorization. This method is limited in that a) names, pronouns, and social media profiles used to construct the databases may ¹³²⁰ not, in every case, be indicative of gender identity and b) it cannot account for intersex, non-binary, or transgender people. We look forward to future work that could help us to better understand how to support equitable practices in science.

References

- [1] Vincent D. Costa, Andrew R. Mitz, and Bruno B. Averbeck. "Subcortical Substrates 1325 of Explore-Exploit Decisions in Primates". In: *Neuron* 103.3 (2019), 533–545.e5.
- [2] Becket R. Ebitz, Eddy Albarran, and Tirin Moore. "Exploration Disrupts Choice-Predictive Signals and Alters Dynamics in Prefrontal Cortex". In: *Neuron* 97 (2 2018), 450–461.e9.
- [3] Theresa M. Desrochers, Dezhe Z. Jin, Noah D. Goodman, and Ann M Graybiel. 1330 "Optimal habits can develop spontaneously through sensitivity to local cost". In: *Proceedings of the National Academy of Sciences* 107.47 (2010), pp. 20512–20517.
- [4] Leslie P. Kaelbling, Michael L. Littman, and Andrew W. Moore. "Reinforcement Learning: A Survey". In: *Journal of Artificial Intelligence Research.* 4 (1996), p. 237.
- [5] Samuel J. Gershman. "Deconstructing the human algorithms for exploration". In: 1335 Cognition 173 (2018), pp. 34–42.
- [6] Theresa M. Desrochers, Ken-ichi Amemori, and Ann M. Graybiel. "Habit Learning by Naive Macaques Is Marked by Response Sharpening of Striatal Neurons Representing the Cost and Outcome of Acquired Action Sequences". In: *Neuron* 87.4 (2015), pp. 853–868.
- [7] Melanie Mitchell. Complexity: A Guided Tour 1st Edition. Oxford University Press, 2011.
- [8] Monica D Rosenberg, Dustin Scheinost, Abigail S Greene, Emily W Avery, Young H Kwon, Emily S Finn, Ramachandran R Ramani, Maolin Qiu, R Todd Constable, and Marvin M Chun. "Functional connectivity predicts changes in attention observed 1345 across minutes, days, and months". In: *Proc Natl Acad Sci U S A* 117.7 (2020), pp. 3797–3807.
- [9] Aron K. Barbey. "Network Neuroscience Theory of Human Intelligence". In: *Trends in Cognitive Sciences* 22.1 (2018), pp. 8–20.
- [10] Manesh Girn, Caitlin Mills, and Kalina Christoff. "Linking brain network reconfiguration and intelligence: Are we there yet?" In: *Trends in Neuroscience and Education* 15 (2019), pp. 62–70.
- [11] Danielle S. Bassett and Marcelo G. Mattar. "A Network Neuroscience of Human Learning: Potential to Inform Quantitative Theories of Brain and Behavior". In:

 Trends in Cognitive Sciences 21.4 (2017), pp. 250–264.
- [12] Danielle S. Bassett, Perry Zurn, and Joshua I. Gold. "On the nature and use of models in network neuroscience". In: *Nature Reviews Neuroscience* 19.9 (2018), pp. 566–578.

- [13] Chang-Hao Kao, Ankit N. Khambhati, Danielle S. Bassett, Matthew R. Nassar, Joseph T. McGuire, Joshua I. Gold, and Joseph W. Kable. "Functional brain 1360 network reconfiguration during learning in a dynamic environment". In: *Nature Communications* 800284 (2019).
- [14] Courtney L. Gallen and Mark D'Esposito. "Brain Modularity: A Biomarker of Intervention-related Plasticity". In: Trends in Cognitive Science 23.4 (2019), pp. 293–304.
- [15] Raphael T. Gerraty, Juliet Y. Davidow, Karin Foerde, Adriana Galvan, Danielle S. Bassett, and Daphna Shohamy. "Dynamic Flexibility in Striatal-Cortical Circuits Supports Reinforcement Learning". In: *Journal of Neuroscience* 38.10 (2018), pp. 2442–2453.
- [16] Danielle S. Bassett, Muzhi Yang, Nicholas F. Wymbs, and Scott T. Grafton. 1370 "Learning-induced autonomy of sensorimotor systems". In: *Nature Neuroscience* 18.5 (2015), pp. 744–751.
- [17] Maxwell A. Bertolero and Danielle S. Bassett. "On the nature of explanations offered by network science: A perspective from and for practicing neuroscientists".

 In: *Topics* Epub Ahead of Print (2019).
- [18] Adilson E. Motter. "Networkcontrology". In: Chaos 25.9 (2015), p. 097621.
- [19] Fabio Pasqualetti, Sandro Zampieri, and Francesco Bullo. "Controllability Metrics, Limitations and Algorithms for Complex Networks". In: *IEEE Transactions on Control of Network Systems* 1.1 (2014), pp. 40–52.
- [20] Yang Y. Liu, Jean J. Slotine, and Albert L. Barabási. "Controllability of complex 1380 networks". In: *Nature* 473.7346 (2011), pp. 167–173.
- [21] Jason Z. Kim and Danielle S. Bassett. "Linear Dynamics and Control of Brain Networks". In: *Neuroengineering*. Ed. by Bin He. Springer, 2020.
- [22] Jennifer Stiso, Ankit N. Khambhati, Tommaso Menara, Ari E. Kahn, Joel M. Stein, Sandihitsu R. Das, Richard Gorniak, Joseph Tracy, Brian Litt, Kathryn A. Davis, 1385 Fanio Pasqualetti, Timothy H. Lucas, and Danielle S. Bassett. "White Matter Network Architecture Guides Direct Electrical Stimulation through Optimal State Transitions". In: Cell Reports 28.10 (2019), 2554–2566.e7.
- [23] Eli J. Cornblath, Evelyn Tang, Graham L. Baum, Tyler M. Moore, Azeez Adebimpe, David R. Roalf, Ruben C. Gur, Raquel E. Gur, Fabio Pasqualetti, Theodore D. 1390 Satterthwaite, and Danielle S. Bassett. "Sex differences in network controllability as a predictor of executive function in youth". In: *Neuroimage* 188 (2019), pp. 122–134.

- [24] Dale Zhou, Yoona Kang, Danielle Cosme, Mia Jovanova, Xiaosong He, Arun Mahadevan, Jeesung Ahn, Ovidia Stanoi, Julia K. Brynildsen, Nicole Cooper, Eli J. Cornblath, Linden Parkes, Peter J. Mucha, Kevin N. Ochsner, David M. 1395 Lydon-Staley, Emily B. Falk, and Dani S. Bassett. "Mindful attention promotes control of brain network dynamics for self-regulation and discontinues the past from the present". In: Proceedings of the National Academy of Sciences 120.2 (2023), e2201074119.
- [25] Gang Yan, Petra E. Vértes, Emma K. Towlson, Yee L. Chew, Denise S. Walker, 1400 William R. Schafer, and Albert L Barabási. "Network control principles predict neuron function in the Caenorhabditis elegans connectome". In: Nature 550.7677 (2017), pp. 519–523.
- [26] Karl J. Friston. "Functional and effective connectivity: A review". In: *Brain Connectivity* 1.1 (2011), pp. 13–36.
- [27] Danai Dima, Karl J. Friston, Klass E. Stephan, and Sophia Frangou. "Neuroticism and conscientiousness respectively constrain and facilitate short-term plasticity within the working memory neural network". In: *Human Brain Mapping* 36.10 (2015), pp. 4158–4163.
- [28] Christian Büchel, J T Coull, and Karl J. Friston. "The predictive value of changes in 1410 effective connectivity for human learning". In: *Science* 283.5407 (1999), pp. 1538–1541.
- [29] Urs Braun, Anais Harneit, Giulio Pergola, Tommaso Menara, Axel Schaefer, Richard F. Betzel, Zhenxiang Zang, Janina I. Schweiger, Xiaolong Zhang, Kristina Schwarz, Junfang Chen, Giuseppe Blasi, Alessandro Bertolino, Daniel Durstewitz, Fabio Pasqualetti, Emanuel Schwarz, Andreas Meyer-Lindenberg, Danielle S. Bassett, 1415 and Heike Tost. "Brain network dynamics during working memory are modulated by dopamine and diminished in schizophrenia". In: *Nature Communications* 12 (2021), p. 3478.
- [30] Christina Savin and Gasper Tkačik. "Maximum entropy models as a tool for building precise neural controls". In: *Current Opinion in Neurobiology* 46 (2017), 1420 pp. 120–126.
- [31] Einat Granot-Atedgi, Gasper Tkačik, R. Segev, and Elad Schneidman. "Stimulus-dependent maximum entropy models of neural population codes". In: *PLoS Computational Biology* 9.3 (2013), e1002922.
- [32] Leenoy Meshulam, J L Gauthier, Carlos D. Brody, David W. Tank, and William 1425 Bialek. "Collective Behavior of Place and Non-place Neurons in the Hippocampal Network". In: *Neuron* 96.5 (2017), 1178–1191.e4.
- [33] Karl Friston, James Kilner, and Lee Harrison. "A free energy principle for the brain". In: *Journal of Physiology Paris* 100 (2006), pp. 70–87.

- [34] Pedro A. Ortega and Daniel A. Braun. "Thermodynamics as a theory of decision-makingo with information-processing costs". In: *Proceedings of the Royal Society A* 469.2012 (2013), p. 0683.
- [35] Raul Vicente, Michael Wibral, Michael Lindner, and Gordon Pipa. "Transfer entropy—a model-free measure of effective connectivity for the neurosciences". In:

 Journal of Computational Neuroscience 30.1 (2011), pp. 45–67.
- [36] Kent Berridge. "From prediction error to incentive salience: mesolimbic computation of reward motivation". In: European Journal of Neuroscience 35.7 (2011), pp. 1124–1143.
- [37] Ann M. Graybiel and Scott T. Grafton. "The Striatum: Where Skills and Habits Meet". In: Cold Spring Harbor Perspectives in Biology 7.8 (2015), a021691.
- [38] Trinity B. Crapse and Marc A. Sommer. "Frontal Eye Field Neurons with Spatial 1440 Representations Predicted by Their Subcortical Input". In: *Journal of Neuroscience* 29.16 (2009), pp. 5308–5318.
- [39] Adam Messinger, Rosella Cirillo, Steven P. Wise, and Aldo Genovesio. "Separable neuronal contributions to covertly attended locations and movement goals in macaque frontal cortex". In: *Science Advances* 7.14 (2021), eabe0716.
- [40] Jacqueline Gottlieb and Pierre Y. Oudeyer. "Towards a neuroscience of active sampling and curiosity". In: *Nature Reviews Neuroscience* 19.12 (2018), pp. 758–770.
- [41] Kyle S. Smith and Ann M. Graybiel. "A Dual Operator View of Habitual Behavior Reflecting Cortical and Striatal Dynamics". In: *Neuron* 79.2 (2013), pp. 361–374.
- [42] Edmond Teng, Lisa Stefanacci, Larry R. Squire, and Stuart M. Zola. "Contrasting 1450 effects on discrimination learning after hippocampal lesions and conjoint hippocampal-caudate lesions in monkeys". In: *The Journal of Neuroscience* 20.10 (2000), pp. 3853–3863.
- [43] Cathy J. Price, Maria LuisaGorno-Tempini, Kim S. Graham, Nora Biggio, Andrea Mechelli, Karalyn Patterson, and Uta Noppeney. "Normal and pathological reading: converging data from lesion and imaging studies". In: *Neuroimage* 20. Supplement 1 1455 (2003), S30–S41.
- [44] Alicia Izquierdo and Elisabeth A. Murray. "Combined unilateral lesions of the amygdala and orbital prefrontal cortex impair affective processing in rhesus monkeys". In: *Journal of Neurophysiology* 94.5 (2004), pp. 2023–2039.
- [45] Terrell A. Jenrette, Jordan B. Logue, and Kristen A. Horner. "Lesions of the Patch 1460 Compartment of Dorsolateral Striatum Disrupt Stimulus-Response Learning". In: *Neuroscience* 415 (2019), pp. 161–172.
- [46] Lina Yassin, Brett L. Benedetti, Jean-Sébastien Jouhanneau, Jing A. Wen, James F.A. Poulet, and Alison L. Barth. "An Embedded Subnetwork of Highly Active Neurons in the Neocortex". In: *Neuron* 68.6 (2010), pp. 1043–1050.

- [47] Marianna Yanike and Vincent P. Ferrera. "Representation of outcome risk and action in the anterior caudate nucleus". In: *Journal of Neuroscience* 34.9 (2014), pp. 3279–3290.
- [48] Hyoung F. Kim, Ali Ghazizadeh, and Okihide Hikosaka. "Dopamine Neurons Encoding Long-Term Memory of Object Value for Habitual Behavior". In: *Cell* 1470 163.5 (2015), pp. 1165–1175.
- [49] Clarissa J. Whitmire and Garrett B. Stanley. "Rapid Sensory Adaptation Redux: A Circuit Perspective". In: *Neuron* 92.2 (2016), pp. 298–315.
- [50] Mona Garvert, Karl J. Friston, Raymond J. Dolan, and Marta I. Garrido. "Subcortical amygdala pathways enable rapid face processing". In: *Neuroimage* 102.2 (2014), 1475 pp. 309–316.
- [51] Hiroshi Makino, Eun J. Hwang, Nathan G. Hedrick, and Takaki Komiyama. "Circuit Mechanisms of Sensorimotor Learning". In: *Neuron* 92.4 (2016), pp. 705–721.
- [52] Julia Cox and Ilana B. Witten. "Striatal circuits for reward learning and decision-making".
 In: Nature Reviews Neuroscience 20.8 (2019), pp. 482–494.
- [53] Elizabeth Litvina, Amy Adams, Alison Barth, Marcel Bruchez, James Carson, Jason E. Chung, Kristin B. Dupre, Loren M Frank, Kathleen M. Gates, Kristen M. Harris, Hannah Joo, Jeff William Lichtman, Khara M. Ramos, Terrence Sejnowski, James S. Trimmer, Samantha White, and Walter Koroshetz. "BRAIN Initiative: Cutting-Edge Tools and Resources for the Community". In: Journal of Neuroscience 1485 39.42 (2019), pp. 8275–8284.
- [54] Joseph Feingold, Theresa M. Desrochers, Naotaka Fujii, Ray Harlan, Patrick L. Tierney, Hideki Shimazu, Ken-Ichi Amemori, and Ann M. Graybiel. "A system for recording neural activity chronically and simultaneously from multiple cortical and subcortical regions in nonhuman primates". In: *Journal of Neurophysiology* 1490 107 (2012), pp. 1979–1995.
- [55] Jason E Chung, Hannah R. Joo, Jiang L. Fan, Daniel F. Liu, Alex H. Barnett, Supin Chen, Charlotte Geaghan-Breiner, Mattias P. Karlsson, Magnus Karlsson, Kye Y. Lee, Hexin Liang, Jeremy F. Magland, Jeanine A. Pebbles, Angela C. Tooker, Leslie F. Greengard, Vanessa M. Tolosa, and Loren M. Frank. "High-Density, 1495 Long-Lasting, and Multi-region Electrophysiological Recordings Using Polymer Electrode Arrays". In: Neuron 101.1 (2019), 21–31.e5.
- [56] Guosong Hong and Charles M. Lieber. "Novel electrode technologies for neural recordings". In: *Nature Reviews Neuroscience* 20.6 (2019), pp. 330–345.

- [57] David Kleinfeld, Lan Luan, Partha P. Mitra, Jacob T. Robinson, Rahul Sarpeshkar, 1500 Kenneth Shepard, Chong Xie, and Timothy D. Harris. "Can One Concurrently Record Electrical Spikes from Every Neuron in a Mammalian Brain?" In: *Neuron* 103.6 (2019), pp. 1005–1015.
- [58] Fjodor Van Veen and Stefan Leijnen. *The Neural Network Zoo.* 2019. URL: https://www.asimovinstitute.org/neural-network-zoo.
- [59] Wolfgang Maass, Thomas Natschlager, and Henry Markram. "Real-time computing without stable states: A new framework for neural computation based on perturbations". In: *Neural computation* 14.11 (2002), pp. 2531–2560.
- [60] Yann LeCun, Léon Bottou, Yoshua Bengio, and Patrick Haffner. "Gradient-based learning applied to document recognition". In: *Proceedings of the IEEE* 86.11 (1998), 1510 pp. 2278–2324.
- [61] Geoffrey E. Hinton and Terrence J Sejnowski. "Learning and relearning in Boltzmann machines". In: *Parallel distributed processing: Explorations in the microstructure of cognition* 1 (1986), pp. 282–317.
- [62] Priyamvada Rajasethupathy, Sethuraman Sankaran, James H. Marshel, Christina K. 1515 Kim, Emily Ferenczi, Soo Y. Lee, Andre Berndt, Charu Ramakrishnan, Anna Jaffe, Maisie Lo, Conor Liston, and Karl Deisseroth. "Projections from neocortex mediate top-down control of memory retrieval". In: *Nature* 526.7575 (2015), pp. 653–659.
- [63] Carino Curto, Anda Degeratu, and Vladimir Itskov. "Flexible memory networks". In: Bulletin of Mathematical Biology 74.3 (2012), pp. 590–614.
- [64] Kanaka Rajan, Christopher D. Harvey, and David W. Tank. "Recurrent Network Models of Sequence Generation and Memory". In: Neuron 90.1 (2016), pp. 128–142.
- [65] Scott T. Murdison, Guillaume Leclercq, Philippe Lefèvre, and Gunnar Blohm. "Computations underlying the visuomotor transformation for smooth pursuit eye movements". In: *Journal of Neurophysiology* 113.5 (2015), pp. 1377–1399.
- [66] Nadav Kashtan and Uri Alon. "Spontaneous evolution of modularity and network motifs". In: Proceedings of the National Academy of Sciences 102.39 (2005), pp. 13773–13778.
- [67] Andrew J. Whalen, Sean N. Brennan, Timothy D. Sauer, and Steven J. Schiff. "Observability and Controllability of Nonlinear Networks: The Role of Symmetry". 1530 In: Physical Review X 5 (2015), p. 011005.
- [68] Brent Doiron, Ashok Litwin-Kumar, Robert Rosenbaum, Gabriel K Ocker, and Krešimir Josić. "The mechanics of state-dependent neural correlations". In: *Nature Neuroscience* 19.3 (2016), pp. 383–393.

- [69] Adam Kohn, Ruben Coen-Cagli, Ingmar Kanitscheider, and Alexandre Pouget. 1535 "Correlations and Neuronal Population Information". In: *Annual Review of Neuroscience* 39 (2016), pp. 237–256.
- [70] Karl J Friston. "Models of brain function in neuroimaging". In: Annual Review of Psychology 56 (2005), pp. 57–87.
- [71] Abdelhak Mahmoudi, Sylvain Takerkart, Fakhita Regragui, Driss Boussaoud, 1540 and Andrea Brovelli. "Multivoxel pattern analysis for FMRI data: a review". In: Computational and Mathematical Methods in Medicine 2012 (2012), p. 961257.
- [72] Gabriel K. Ocker, Krešimir Josić, Eric Shea-Brown, and Michael A. Buice. "Linking structure and activity in nonlinear spiking networks". In: *PLoS Computational Biology* 13.6 (2017), e1005583.
- [73] Jannis Schuecker, Maximilian Schmidt, Sacha J. van Albada, Markus Diesmann, and Moritz Helias. "Fundamental Activity Constraints Lead to Specific Interpretations of the Connectome". In: *PLoS Computational Biology* 13.2 (2017), e1005179.
- [74] Takuya Ito, Luke Hearne, Ravi Mill, Carrisa Cocuzza, and Michael W. Cole. "Discovering the Computational Relevance of Brain Network Organization". In: 1550 Trends in Cognitive Sciences S1364–6613.19 (2019), pp. 30240–2.
- [75] Michael Breakspear. "Dynamic models of large-scale brain activity". In: *Nature Neuroscience* 20.3 (2017), pp. 340–352.
- [76] Huawei Fan, Yafeng Wang, Kai Yang, and Xingang Wang. "Enhancing network synchronizability by strengthening a single node". In: *Physical Review E* 99.4–1 1555 (2019), p. 042305.
- [77] Francesco Sorrentino, Louis M. Pecora, Aaron M. Hagerstrom, Thomas E. Murphy, and Rajarshi Roy. "Complete characterization of the stability of cluster synchronization in complex dynamical networks". In: *Science Advances* 2.4 (2016), e1501737.
- [78] Tommaso Menara, Giacomo Baggio, Danielle S. Bassett, and Fabio Pasqualetti. 1560 "Stability Conditions for Cluster Synchronization in Networks of Heterogeneous Kuramoto Oscillators". In: *IEEE Transactions on Control of Network Systems* 7.1 (2020), pp. 302–314.
- [79] Antonio Ortega, Pascal Frossard, Jelena Kovačević, José M. F. Moura, and Pierre Vandergheynst. "Graph Signal Processing: Overview, Challenges, and Applications". 1565 In: *Proceedings of the IEEE* 106.5 (2018), pp. 808–828.
- [80] Weiyu Huang, Thomas A. W. Bolton, John D. Medaglia, Danielle S. Bassett, Alejandro Ribeiro, and Dimitri Van De Ville. "A Graph Signal Processing Perspective on Functional Brain Imaging". In: *Proceedings of the IEEE* 106.5 (2018), pp. 868–885.

- [81] Sandip Roy, Terry F. McElwain, and Yan Wan. "A network control theory approach 1570 to modeling and optimal control of zoonoses: case study of brucellosis transmission in sub-Saharan Africa". In: *PLoS Neglected Tropical Diseases* 5.10 (2011), e1259.
- [82] Ernest Barany, Steve Schaffer, Kevin Wedeward, and Steven Ball. "Nonlinear controllability of singularly perturbed models of power flow networks". In: *IEEE Conference on Decision and Control* 5 (2004), pp. 4826–4832.
- [83] Michael X. Henderson, Eli J. Cornblath, Adam Darwich, Bin Zhang, Hannah Brown, Ronald J. Gathagan, Raizel M. Sandler, Danielle S. Bassett, John Q. Trojanowski, and Virginia M. Y. Lee. "Spread of α-synuclein pathology through the brain connectome is modulated by selective vulnerability and predicted by network analysis". In: *Nature Neuroscience* 22.8 (2019), pp. 1248–1257.
- [84] Boris C. Bernhardt, Fatemeh Fadaie, Min Liu, Benoit Caldairou, Shi Gu, Elizabeth Jefferies, Jonathan Smallwood, Danielle S. Bassett, Andrea Bernasconi, and Neda Bernasconi. "Temporal lobe epilepsy: Hippocampal pathology modulates connectome topology and controllability". In: *Neurology* 92.19 (2019), e2209–e2220.
- [85] Emma K. Towlson, Petra E. Vertes, Gang Yan, Yee L. Chew, Denise S. Walker, 1585 William R. Schafer, and Albert L. Barabasi. "Caenorhabditis elegans and the network control framework-FAQs". In: *Philosophical Transactions of the Royal Society of London. Series B, Biological Sciences.* 373.1758 (2018).
- [86] Steven Schiff. Neural Control Engineering. MIT Press, 2011.
- [87] Jayson Jeganathan, Alistair Perry, Danielle S. Bassett, Gloria Roberts, Philip B. 1590 Mitchell, and Michael Breakspear. "Fronto-limbic dysconnectivity leads to impaired brain network controllability in young people with bipolar disorder and those at high genetic risk". In: *Neuroimage Clinical* 19 (2018), pp. 71–81.
- [88] João P. Hespanha. *Linear systems theory*. Princeton University Press, 2018.
- [89] Vladimir G. Boltyanskii, Revaz V. Gamkrelidze, and Lev S. Pontryagin. *The theory* 1595 of optimal processes. I. The maximum principle. 1960.
- [90] Erfan Nozari, Maxwell A Bertolero, Jennifer Stiso, Lorenzo Caciagli, Eli J Cornblath, Xiaosong He, Arun S Mahadevan, George J Pappas, and Dani S Bassett. "Macroscopic resting-state brain dynamics are best described by linear models". In: *Nature Biomedical Engineering* (2023).
- [91] Thomas Kailath. *Linear Systems*. Prentice-Hall, 1980.
- [92] Siby J. Plathottam and Hossein Salehfar. "Transient Loss Minimization in Induction Machine Drives using Optimal Control Theory". In: *IEEE International Electric Machines & Drives Conference* (2015), pp. 1744–1780.

- [93] Ali M. Sahlodin and Paul I. Barton. "Efficient Control Discretization Based on 1605 Turnpike Theory for Dynamic Optimization". In: *Processes* 5 (2017), p. 85.
- [94] Thomas J Boehme, Florian Held, Matthias Schultalbers, and Bernhard Lampe.
 "Trip-based energy management for electric vehicles: An optimal control approach".
 In: American Control Conference 2013 (2013), pp. 5978–5983.
- [95] Theodore L. Sourkes. "On the energy cost of mental effort". In: *Journal of the* 1610 *History of the Neurosciences* 15.1 (2006), pp. 31–47.
- [96] Adrian M. Heith and John W. Krakauer. "The multiple effects of practice: skill, habit and reduced cognitive load". In: Current Opinion in Behavioral Sciences 20 (2018), pp. 196–201.
- [97] Agnes Moors and Jan D. Houwer. "Automaticity: A Theoretical and Conceptual 1615 Analysis". In: *Psychological Bulletin* 132.2 (2006), pp. 297–326.
- [98] Yoshiki Iwamoto and Yuki Kaku. "Saccade adaptation as a model of learning in voluntary movements". In: Experimental Brain Research 204.2 (2010), pp. 145–162.
- [99] Theresa M. Desrochers, Christopher H. Chatham, and David Badre. "The Necessity of Rostrolateral Prefrontal Cortex for Higher-Level Sequential Behavior". In: *Neuron* 1620 87.6 (2015), pp. 1357–1368.
- [100] David Badre, Bradley B. Doll, Nicole M. Long, and Michael J. Frank. "Rostrolateral prefrontal cortex and individual differences in uncertainty-driven exploration". In: *Neuron* 73.3 (2012), pp. 595–607.
- [101] Carol A. Seger and Corinna M. Cincotta. "The Roles of the Caudate Nucleus 1625 in Human Classification Learning". In: *Journal of Neuroscience* 25.11 (2005), pp. 2941–2951.
- [102] Carol A. Seger. "The Involvement of Corticostriatal Loops in Learning Across Tasks, Species, and Methodologies". In: *The Basal Ganglia IX*. Ed. by H. Jan Groenewegen, P. Voorn, H. W. Berendse, A. B. Mulder, and A. R. Cools. Springer, 1630 2009, pp. 25–39.
- [103] William R. Schafer. "The Worm Connectome: Back to the Future". In: *Trends in Neurosciences* 41.11 (2018), pp. 763–765.
- [104] Katharina Eichler, Feng Li, Ashok Litwin-Kumar, Youngser Park, Ingrid Andrade, Casey M. Schneider-Mizell, Timo Saumweber, Annina Huser, Claire Eschbach, 1635 Bertram Gerber, Richard D. Fetter, James W. Truman, Carey E. Priebe, L. F. Abbott, Andreas S. Thum, Marta Zlatic, and Albert Cardona. "The complete connectome of a learning and memory centre in an insect brain". In: Nature 548.7666 (2017), pp. 175–182.

- [105] Elizabeth M. C. Hillman, Venkatakaushik Voleti, Wenze Li, and Hang Yu. "Light-Sheet640 Microscopy in Neuroscience". In: *Annual Review of Neuroscience* 42 (2019), pp. 295–313.
- [106] Anna L. Eberle, Olaf Selchow, Marlene Thaler, Dirk Zeidler, and Robert Kirmse. "Mission (im)possible mapping the brain becomes a reality". In: *Microscopy* 64.1 (2015), pp. 45–55.
- [107] Daniel R. Berger, H. S. Seung, and Jeff W. Lichtman. "VAST (Volume Annotation 1645 and Segmentation Tool): Efficient Manual and Semi-Automatic Labeling of Large 3D Image Stacks". In: Frontiers in Neural Circuits 12 (2018), p. 88.
- [108] Gaia Tavoni, Simona Cocco, and Remi Monasson. "Neural assemblies revealed by inferred connectivity-based models of prefrontal cortex recordings". In: *Journal of Computational Neuroscience* 41.3 (2016), pp. 269–293.
- [109] Jonathan Schiefer, Alexander Niederbühl, Volker Pernice, Carolin Lennartz, Jürgen Hennig, Pierre LeVan, and Stefan Rotter. "From correlation to causation: Estimating effective connectivity from zero-lag covariances of brain signals". In: *PLoS Computational Biology* 14.3 (2018), e1006056.
- [110] Arseny A. Sokolov, Peter Zeidman, Michael Erb, Philippe Ryvlin, Marina A. 1655 Pavolva, and Karl J. Friston. "Linking structural and effective brain connectivity: structurally informed Parametric Empirical Bayes (si-PEB)". In: *Brain Structure* and Function 224 (1 2019), pp. 205–217.
- [111] Alessandro Crimi, Luca Dodero, Fabio Sambataro, Vittorio Murino, and Diego Sona. "Structurally constrained effective brain connectivity". In: *Neuroimage* 239 1660 (2021), p. 118288.
- [112] Brittany H. Scheid, Arian Ashourvan, Jennifer A. Stiso, Kathryn A. Davis, Fadi Mikhail, Fabio Pasqualetti, Brian Litt, and Danielle S. Bassett. "Time-evolving controllability of effective connectivity networks during seizure progression". In:

 Proceedings of the National Academy of Sciences 118.5 (2021), e2006436118.
- [113] Demian Battaglia, Annette Witt, Fred Wolf, and Theo Geisel. "Dynamic effective connectivity of inter-areal brain circuits". In: *PLoS Computational Biology* 8.3 (2012), e1002438.
- [114] Christopher J. Honey, Olaf Sporns, Leila Cammoun, Xavier Gigandet, Jean-Philippe Thiran, Reto Meuli, and Patric Hagmann. "Predicting human resting-state functional connectivity from structural connectivity". In: *Proceedings of the National Academy of Sciences* 106.6 (2009), pp. 2035–2040.
- [115] Xiaosong He, Lorenzo Caciagli, Linden M Parkes, Jennifer Stiso, Teresa M Karrer, Jason Z Kim, Zhixin Lu, Tommaso Menara, Fabio Pasqualetti, Michael R Sperling, et al. "Pathological and metabolic underpinnings of energetic inefficiency in 1675 temporal lobe epilepsy". In: bioRxiv (2021).

- [116] Alan Leshner and Donal W. Pfaff. "Quantification of behavior". In: *Proceedings of the National Academy of Sciences* 108. Supplement 3 (2011), pp. 15537–15541.
- [117] Marie E. Bellet, Joachim Bellet, Hendrikje Nienborg, Ziad M. Hafed, and Phillip Berens. "Human-level saccade detection performance using deep neural networks". 1680 In: *Journal of Neurophysiology* 121.2 (2019), pp. 646–661.
- [118] Alexander Belyi, Iva Bojic, Stanislav Sobolevsky, Izabela Sitko, Bartosz Hawelka, Lada Rudikova, Alexander Kurbatski, and Carlo Ratti. "Global multi-layer network of human mobility". In: *International Journal of Geographical Information Science* 31.7 (2017), pp. 1381–1402.
- [119] Robert X.D. Hawkins, Noah D. Goodman, and Robert L. Goldstone. "The Emergence of Social Norms and Conventions". In: *Trends in Cognitive Sciences* 23.2 (2019), pp. 158–169.
- [120] Peter Wills and Francois G. Meyer. "Metrics for Graph Comparison: A Practitioner's Guide". In: arXiv 1412 (2019), p. 2447.
- [121] Benoit Mandelbrot. *The Fractal Geometry of Nature*. W. H. Freeman and Company, 1983.
- [122] Philip M. Iannaccone and Mustafa Khokha. Fractal Geometry in Biological Systems. CRC Press, 1996.
- [123] Thomas G. Smith, G D Lange, and William B. Marks. "Fractal methods and results 1695 in cellular morphology dimensions, lacunarity and multifractals". In: *Journal of Neuroscience Methods* 69.2 (1996), pp. 123–136.
- [124] Jing Z. Liu, Lu D. Zhang, and Guang H. Yue. "Fractal Dimension in Human Cerebellum Measured by Magnetic Resonance Imaging". In: *Biophysical Journal* 85.6 (2003), pp. 4041–4046.
- [125] Chaoming Song, Shlomo Havlin, and Hernán A. Makse. "Self-similarity of complex networks". In: *Nature* 433.7024 (2005), pp. 392–395.
- [126] Jian Li, Qian Du, and Caixin Sun. "An improved box-counting method for image fractal dimension estimation". In: *Pattern Recognition* 42.11 (2009), pp. 2460–2469.
- [127] Lior Rokach and Oded Z. Maimon. "Clustering methods". In: Data mining and 1705 knowledge discovery handbook. Ed. by L Rokach and O Maimon. Springer, 2005, pp. 321–352.
- [128] Ad Aertsen and Hubert Preissl. "Dynamics of activity and connectivity in physiological neuronal networks". In: *Nonlinear dynamics and neuronal networks*. Ed. by H G Schuster. VGH, 1991, pp. 281–302.

- [129] Jennifer Stiso, Marie-Constance Corsi, Jean M. Vettel, Javier Garcia, Fabio Pasqualetti, Fabrizio De Vico Fallani, Timothy H. Lucas, and Danielle S. Bassett. "Learning in brain-computer interface control evidenced by joint decomposition of brain and behavior". In: ournal of Neural Engineering 4 (2020), p. 046018.
- [130] Tommaso Menara, Giacomo Baggio, Danielle S. Bassett, and Fabio Pasqualetti. 1715
 "A Framework to Control Functional Connectivity in the Human Brain". In: 2019
 IEEE 58th Conference on Decision and Control (CDC) (2019), pp. 4697–4704.
- [131] Shinya Ito, Michael E. Hansen, Randy Heiland, Andrew Lumsdaine, Alan M. Litke, and John M. Beggs. "Extending Transfer Entropy Improves Identification of Effective Connectivity in a Spiking Cortical Network Model". In: *PLoS One* 6.11 1720 (2011), e27431.
- [132] Richard F. Betzel, Shi Gu, John D. Medaglia, Fabio Pasqualetti, and Danielle S. Bassett. "Optimally controlling the human connectome: the role of network topology". In: *Scientific Reportes* 6 (2016), p. 30770.
- [133] Charles J. Bruce and Michael E. Goldberg. "Primate frontal eye fields. I. Single 1725 neurons discharging before saccades". In: *Journal of Neurophysiology* 53.3 (1985), pp. 603–635.
- [134] Sara McLaughlin Mitchell, Samantha Lange, and Holly Brus. "Gendered Citation Patterns in International Relations Journals1". In: *International Studies Perspectives* 14.4 (2013), pp. 485–492. ISSN: 1528-3577. DOI: 10.1111/insp.12026. URL: https://doi.org/10.1111/insp.12026.
- [135] Michelle L. Dion, Jane Lawrence Sumner, and Sara McLaughlin Mitchell. "Gendered Citation Patterns across Political Science and Social Science Methodology Fields". en. In: Political Analysis 26.3 (July 2018), pp. 312–327. ISSN: 1047-1987, 1476-4989. DOI: 10.1017/pan.2018.12. URL: https://www.cambridge.org/core/1735product/identifier/S1047198718000128/type/journal_article (visited on 08/22/2019).
- [136] Neven Caplar, Sandro Tacchella, and Simon Birrer. "Quantitative evaluation of gender bias in astronomical publications from citation counts". en. In: *Nature Astronomy* 1.6 (June 2017), p. 0141. ISSN: 2397-3366. DOI: 10.1038/s41550-017-1740 0141. URL: http://www.nature.com/articles/s41550-017-0141 (visited on 08/22/2019).
- [137] Daniel Maliniak, Ryan Powers, and Barbara F. Walter. "The Gender Citation Gap in International Relations". en. In: International Organization 67.4 (Oct. 2013), pp. 889–922. ISSN: 0020-8183, 1531-5088. DOI: 10.1017/S0020818313000209. URL:1745 https://www.cambridge.org/core/product/identifier/S0020818313000209/type/journal_article (visited on 08/22/2019).

- [138] Jordan D. Dworkin, Kristin A. Linn, Erin G. Teich, Perry Zurn, Russell T. Shinohara, and Danielle S. Bassett. "The extent and drivers of gender imbalance in neuroscience reference lists". In: Nature Neuroscience (2020). DOI: 10.1038/s41593-1750 020-0658-y.
- [139] Dale Zhou, Eli J. Cornblath, Jennifer Stiso, Erin G. Teich, Jordan D. Dworkin, Ann S. Blevins, and Danielle S. Bassett. *Gender diversity statement and code notebook* v1.0. 2020.